Volumetric Wear Assessment and Characterization of Striated Pattern of Retrieved UHMWPE Tibial Inserts

BY

ELMIRA MOSLEMI RAD

M.S., Shahid Bahonar University of Kerman, Iran, 2009

THESIS

Submitted as a partial fulfillment of the requirements
for the degree of Master of Science in Bioengineering
in the Graduate College of the
University of Illinois at Chicago, 2015

Chicago, Illinois

DEFENSE COMMITTEE:

Dr. Thomas Royston, Chair

Dr. Markus A. Wimmer, Orthopedics, Rush University, Advisor

Dr. Hannah J. Lundberg, Orthopedics, Rush University

DEDICATION

I would like to dedicate this thesis to my family and friends. My mother who always has encouraged me and supported me for having the opportunity to continue my graduate studies. I would also like to dedicate this thesis to the students and faculty members for their mentorship and help, and the facilities provided by Rush University.

ACKNOWLEDGMENTS

There are many individuals who have contributed greatly to the success of this work. Firstly, I sincerely appreciate my supervisor Dr. Markus A. Wimmer for his guidance and profound expertise throughout these years. Dr. Robin Pourzal for his great assistance and his insight throughout this project. I would like to acknowledge Dr. Michel Laurent and Dr. Hannah Lundberg. They were always willing to answer my questions, provide valuable advice and support in difficulties during the study.

Secondly, I would like to thank Christopher Knowlton, BS for his help and lessons on using autonomous mathematical reconstruction algorithm. I would also like to thank Dr. Yifeng Liao from Northwestern University for his help in conducting Raman spectroscopy. I would also like to thank Dr. Neil Blair from the Northwestern University, Evanston, IL for his great help to perform FTIR on my samples and his patience throughout testing.

I would like to thank NIH for providing funding, The University of Illinois at Chicago, Department of Bioengineering and Rush University for providing funding and lab space while conducting experiments.

TABLE OF CONTENTS

TABLE OF CONTENTS (continued)

LIST OF TABLES

LIST OF FIGURES

LIST OF FIGURES (continued)

Figure Page

LIST OF FIGURES (continued)

Figure Page

LIST OF ABBREVIATIONS

AP	Anterior-Posterior
ATR	Attenuated Total Reflectance
BMI	Body Mass Index
CAD	Computer-aided Design
CDC	Centers of Disease Control and Prevention
CMM	Coordinate Measuring Machine
CoCrMo	Cobalt Chromium Molybdenum
CR	Cruciate Retaining
CRS	Confocal Raman System
DSC	Differential Scanning Calorimetry
EtO	Ethylene Oxide
FB	Fixed Bearing
FTIR	Fourier Transform Infrared
FWHM	full-width at half-maximum
Ge	Germanium
IR	Infrared
MB	Mobile Bearing
MG	Miller Galante
Micro-CT	Micro Computed Tomography
ML	Medial-Lateral
PE	Polyethylene
TEM	Transmission Electron Microscopy
THR	Total Hip Replacement
TKR	Total Knee Replacement
UHMWPE	Ultra High Molecular Weight Polyethylene
XLPE	Cross Linked Polyethylene
ZnSe	Zinc selenide

SUMMARY

Wear debris from ultra high molecular weight polyethylene (UHMWPE) is an important factor that limits the longevity of total knee replacements (TKRs). Due to the complicated geometry of contemporary tibial inserts it is difficult to assess the generated wear volume on retrieved implants accurately. Therefore, quantifying the surface damage on retrieved tibial inserts is critical to improve implant designs. Patient factors such as age, gender, height and weight can affect the wear rate of the insert and longevity of the implant. Furthermore, it is important to understand the occurrence of specific wear features such as striated patterns. These wear features occur frequently and are suspected to alter the wear behavior of the implant. Thus, a better understanding of surface changes related to structural alterations of the polyethylene molecules is crucial.

This study was conducted under two specific aims. The first aim was the determination of the accurate *in vivo* wear rate of the tibial articulation in TKR. An autonomous mathematical reconstruction algorithm was applied to quantify the wear volume change and maximum linear penetration of a collection of 81 TKR retrieved UHMWPE NexGen cruciate-retaining tibial inserts (Zimmer, Warsaw, IN) with an average time *in situ* of 5.27±2.89 years. Metrology data for the surfaces of the tibial inserts were obtained with a coordinate measuring machine (SmartScope, OGP, Inc., Rochester, NY) by scanning the articulating surface with about 400,000 points using a low incident laser. The first hypothesis was that maximum linear penetration can be a good surrogate for wear volume. In part 2 of this aim, patient factors such as age, gender, height and weight were available for 67 out of 81 patients to investigate the impact of these factors on wear rate.

The second aim was to determine the impact of the striated pattern the on UHMWPE wear and to characterize its structure and crystalinity with different microscopic techniques. The first hypothesis for this aim was that the area of striated patterns can be an indicator for higher wear volume loss and linear penetration of retrieved tibial inserts. The striated patterns were observed on 61 of retrieved tibial inserts and the areas were mapped for each medial and lateral side using a CMM. The second hypothesis of this aim was that the hills of the striated pattern have a higher crystallinity compared to the troughs. Two methods, Raman spectroscopy and attenuated total reflectance-Fourier transform infrared spectroscopy (ATR-FTIR), were used to characterize the microstructure of these features on the articulating surface of representative retrieved tibial inserts.

The results suggest that penetration was not an accurate surrogate measure for wear volume of individual TKR polyethylene components but could be utilized large cohorts. Also, by considering age, gender, and weight, only patient weight has a significant impact on the wear rate. The results in second aim demonstrated that the occurance of the striated pattern is not an indicator for high wear, although regression analysis indicated a small increase in wear with striated area. Also, according to Raman, there was a crystallinity change within the striated pattern with the hills have a higher crystallinity than the troughs. Unfortunately the results were not confirmed using ATR-FTIR, likely due to an appropriate magnification.

Keywords: *Total knee replacement, UHMWPE, Wear, Implant retrieval, Crystallinity, Striation, Raman, FTIR*

Chapter 1. Introduction

According to the Centers of Disease Control and Prevention (CDC) there were 719,000 primary TKR performed in the US alone in 2010. This number has been projected to increase to over 1,300,000 by 2020 [1]. Thus, it is of great importance to ensure longevity of such total knee replacement devices.

1.1 Failure of Total Knee Replacement

The performance and longevity of a total knee replacement is crucial especially in younger, heavier and active patients. The increasing demand for TKRs in recent decades will also lead to more frequently occurring revision surgeries which are more expensive and complicated compared to the primary operation. Factors such as infection, UHMWPE failure, fracture, loosening, joint stiffness, tibiofemoral instability, patellar complications, etc. may lead to TKR failure. The most common reasons of TKR device failure are infection, loosening and patellar complications [2,3].

The short term failure of the TKR device can be due to infection, instability and patellafemoral problems that mostly happen within five years *in situ* [3]. In this case, 25% of the components can be infected within the first two year time *in situ* and only 7.8% of components can be infected over two years implantation duration [2].

For the long term failure, aseptic loosening which is the weakness of the bone and implant interface can be a dominant reason for failure. Various factors can cause this failure such as patient activity level, surgical technique, implant material and its design. Although due to the improvement of the material and design of the inserts in recent years, the amount of generated wear reduces [4], still the wear particles of UHMWPE in TKRs are a major source of inducing aseptic loosening and consequently the failure of the implant [2,4–7].

Over the last two decades there have been great advances in the design of TKRs, especially in the articulating surface makes its volumetric wear assessment challenging [8–10]. Material properties resulting in lower polyethylene wear. However, to date there is only very little data available on accurately measured volumetric *in vivo* wear rates of contemporary TKR designs. Volumetric wear rates are well established for total hip replacements (THR); however, the more complicated shape of tibial insert makes it more challenging.

1.2 Wear of the Polyethylene Plateau

Quantifying the surface damage in tibial retrievals is critical to improve future implant designs. Therefore, thorough retrieval analysis was performed and a unique metrology method [11] applied to assess the volumetric wear of a collection of TKR retrievals from the retrieval repository at Rush University Medical Center, Chicago, IL, USA.

Aside from implant designs, materials and surgical techniques, patient factors can affect the wear rate of the insert and longevity of the implant. For example, variables such as patient age, gender, height and BMI (Body Mass Index) can have an impact on the survivorship of the implant [2,12,13]. Each factor has a high degree of variability and cannot be considered singularly for investigation of any correlation to wear rate.

1.3 Striated Wear Features

Hood et al., [14] established a semi-quantitative method to score the damage modes and their prevalence in the UHMWPE articulating surface. By characterizing the surface damage it would be possible to investigate the mechanical degradation of implants.

The presence of striated patterns on retrieved tibial inserts have been observed in several studies [15,16], but there is little knowledge how these surface changes relate to changes in

molecular structure of UHMWPE. Wimmer et al. [15], reported on the observation of striated patterns on retrieved tibial inserts relatively early on post-implantation. It has been suggested that the contact mechanics of the knee might be responsible for its generation; thus, the pattern may play an important role in understanding the evolution of surface disruption on the tibial articulation which can lead to more severe damage of the tibial insert [15]. Therefore, the crystallinity change of these features was calculated to analyze the structure and impact of the striated pattern on wear.

1.4 Research Aims and Questions

In this study, two specific aims have been investigated as follow:

Specific Aim 1. Determine accurate *in vivo* wear rate for TKR.

In this aim, polyethylene wear was assessed for retrieved tibial inserts of a single cruciate retaining TKR design (NexGen CR, Zimmer Inc., Warsaw, IN). The retrievals were collected at Rush University Medical Center throughout 2000 to 2012. Metrology data for the surface of the tibial inserts was obtained with a coordinate measuring machine (SmartScope, OGP, Inc., Rochester, NY) and data points were gathered to reconstruct the articular surface of inserts utilizing a novel established autonomous mathematical reconstruction method [11]. In this aim two hypotheses were investigated.

Research question 1: Is maximum linear penetration an accurate surrogate for wear volume?

To answer this question, the maximum linear penetration and the volume loss were calculated for the lateral and medial sides separately for each insert.

Hypothesis: Maximum linear penetration can be an accurate surrogate for wear volume.

Research question 2: Which patient factors impact wear?

Factors such as age, gender and weight/BMI were available for the subgroup of 67 patients to determine if any of these factors can affect the wear rate.

Hypothesis: Generated wear of UHMWPE in tibial inserts of TKRs is higher in younger, heavier male patients.

Specific Aim 2. Determine the polyethylene structure of the striated pattern and its impact on the wear behavior of the insert.

Analyzing the striated features can be helpful to understand the surface disruption on the tibial articulation and the leading causes of severe damage of the tibial inserts.

Research question 1: Is the area of striated pattern an indicator for wear volume loss and maximum linear penetration?

For this aim, the striated patterns were observed on 61 retrieved tibial inserts and also the area of the striation was measured for each medial and lateral tibial plateau for further investigation with wear volume loss and maximum linear penetration.

Hypothesis: The area of striated patterns can be an indicator for wear volume loss and maximum linear penetration of retrieved tibial inserts.

Research question 2: What are the microstructural features of the striated patterns?

In this aim, Raman spectroscopy and ATR-FTIR technique were used to investigate the structure of the striated patterns, to determine if the hill and trough of the striation has different crystallinity.

Hypothesis: The hill in the striated pattern has higher crystallinity compared to the trough due to the rearrangement of the molecules in the articulating surface of the UHMWPE inserts. When mechanical forces are applied, striated patterns are formed.

Chapter 2. Background

The knee joint is one of the strongest and largest joints in the human body that is formed by the tibia (the upper end of the lower leg bone), femur (lower end of the thighbone) and the patella that runs alongside the tibia. The biomechanics of knee joint is extremely complex due to six degrees of freedom. The top of the tibia is covered with cartilage, which is a smooth tissue that provides perfect sliding conditions. The meniscus is also a cartilage tissue and provides shock absorbance and secondary constraint for the joint. The synovium is a smooth tissue that surrounds the knee joint and produces synovial fluid, which acts as a lubricant to reduce the friction in the joint. Degeneration of the cartilage due to various reasons such as infection, arthritis and injury can cause pain and stiffness in the joint. Depending on the extent of damage, patients can suffer from pain and also have difficulty in motion. Medical treatment can help patients to resume their normal daily activities and relieve pain. In the extreme case of pain and impaired function of the native knee joint, an artificial joint such as total knee replacement devices can be a solution [17,18].

2.1 Total Knee Replacement

Total knee replacement (TKR) is one of the most common and successful surgical procedures to relieve knee pain and maintain daily activity. During TKR surgery, destroyed or worn-out surfaces will be replaced with new, uniform surfaces made from artificial materials. These include metal parts which replace the damaged end of the femoral bone and its cartilage and plastic inserts with a metal stem used to replace the end of the tibial plateau. Both metal and plastic components are shaped to restore knee movement and function [18].

2.1.1 Function and Components

The total knee replacement consists of two components which articulate against each other and are designed to provide low friction to restore the smooth motion in the natural knee joint. The bicondylar metal component for the femoral surface is usually made from cobalt-chromium-molybdenum (CoCrMo) alloy or titanium alloy. The tibial insert surface is made from UHMWPE. In contemporary TKR designs the medial and lateral articulating surface of the insert are designed with a dish shape to provide semi-conforming contact conditions. UHMWPE is chosen to provide low friction and good wear performance. A total knee replacement system is shown in Figure 2.1. The prosthesis can be designed to be attached to the bone with bone cement or with porous surfaces on the stem of the prosthesis to allow bone ingrowths [17].

Figure 2.1 Total knee system (NexGen CR, Zimmer Inc., Warsaw, IN).

2.1.2 Ultra High Molecular Weight Polyethylene

Ultra High Molecular Weight Polyethylene (UHMWPE) is a linear polymer of carbon backbones and hydrogen subgroups with molecular weight ranges from 4 to 6 million g/mol. Unique material properties of UHMWPE such as biocompatibility, abrasion resistance, low coefficient of friction, high toughness, corrosion and degradation resistance and also resistance to cyclic fatigue, lead to a wide use in orthopedics implants [19–21].

Ultra high molecular weight polyethylene is a semicrystalline polymer consists of two main regions of 50% crystalline (highly ordered) and 50% amorphous (highly disordered). The crystalline phase primarily consists of orthorhombic structures but monoclinic crystals can be formed under certain conditions such as uniaxial deformation. The size of lamella in the crystalline phase has a thickness of 10-50 nm with a length of 10-50 μm, the lamellae are randomly dispersed within the amorphous phase and bonded with tie molecules [22–24]. There are large numbers of tie molecules in UHMWPE that makes it different from regular high density polyethylene (HDPE). These tie molecules can act as cross-linkers between crystalline regions and improves the load bearing and reduces the contact stress between articulating surfaces, and also improves the chemical and physical strength of polymer [20,25].

The performance of the polyethylene can be affected by various factors, such as, manufacturing method, sterilization method, design, etc. In the following section the various methods for fabrication and sterilization of the UHMWPE are explained.

2.1.2.1 Fabrication of Ultra High Molecular Weight Polyethylene

As mentioned earlier, the manufacturing method is another variable that plays an important role in the performance and longevity of UHMWPE inserts. The two most common methods of medical grade UHMWPE fabrication are compression molding and ram extrusion

[19,26]. For the compression molding method, the UHMWPE components can be generated by machining of sheet material which was press molded from the polyethylene powder or directly by compression of the polyethylene powder to the specific shape and geometry of the component without machining marks on the articulating surface under controlled temperature and pressure [19,26]. In the ram extrusion method, the bar stock can be produced by continuously feeding the polyethylene powder in to a heated cylinder of a ram extruder and the powder is forced into the die by reciprocating ram [19,26]. Thus, the mechanical properties of UHMWPE can be affected by the manufacturing methods and condition of the processing.

2.1.2.2 Sterilization of Ultra High Molecular Weight Polyethylene

Sterilization of any implant material is crucial to prevent any bacteria, fungal or viral contents to be a cause of failure of the implant due to infection. The common techniques for sterilization are Gamma irradiation, Gas Plasma and Ethylene Oxide (EtO). The molecular structure of the polymer can be affected differently by any of these sterilization methods which vary on the rates and dosages of the sterilization techniques [19,27].

Gamma radiation in air with a nominal dose of 2.5 Mrad was a common method of sterilization starting from the 1960s. However, gamma radiation sterilization in air leaves the material prone to oxidation. The physical dose rate can affect the oxygen diffusion to the polymer, and the oxygen can penetrate the molecular structure and react with the free radicals that are created by the ionizing radiation. Oxidative degradation can deteriorate the properties of polymers, such as reducing the tensile strength and other physicals properties. Therefore fatigue wear modes such as delamination and cracking can be generated in the UHMWPE. In high dose rate, oxygen cannot diffuse to polymer fast enough therefore there would be less free radicals to

be reacted. Since 1995, gamma radiation in an inert and oxygen-free environment has been developed to reduce the degradation of UHMWPE due to oxidation [19,27,28].

Gas plasma sterilization is a new surface sterilization method that applies a low temperature of iodized gas. The plasma can be generated in a closed chamber by using the radio frequency of microwave energy to excite the molecules and generate the charged particles in forms of extensively reactive free radicals. Therefore, by attaching to the cell components like enzymes, it deactivates biological organisms [19,27,28]. Due to the shorter sterilization cycle and also nonhazardous byproducts, the gas sterilization technique becomes an attractive sterilization method.

The EtO sterilization technique has been commercially available since the 1970s. EtO is a highly toxic gas which eliminates all life forms and thus can be used to prevent infection. The advantage of this method for UHMWPE is that there are no active constituents of this polymer which can react with EtO and therefore this technique does not affect the physical, chemical and mechanical properties of UHMWPE [27].

The advantage of gas plasma and EtO sterilization methods is that there are no free radicals generated to cause any oxidation. In contrast, gamma radiation may induce cross-linking which is beneficial to strengthen the polyethylene mechanically and its wear resistance [27].

Consequently, sterilization techniques can play an important role in the long term clinical outcomes of UHMWPE.

2.2 Wear and Degradation of Ultra High Molecular Weight Polyethylene Components

Wear particles can be generated from different material sources such as polyethylene, metal, cement, etc. In TKR, the majority of wear particles is generated from the UHMWPE

insert due to wear. These particles may have clinical consequences, which can limit the functional life of a knee replacement. The clinical failure of the knee arthroplasty is frequently due to the release of certain size range and excessive amount of wear particles which cannot be cleared from the joint space. These particle retain within the macrophages of the surrounding tissues and stimulate them to resorb the periprosthetic bone and consequently cause the loosening of the knee replacement that needs the reoperation [29,30].

There are various factors that influence the generation of the wear particles in the artificial prosthesis, such as type of motion, the number of cycles of the motion, patient specific weight and activity level, component design, material parameters, biological environment, etc. [30,31]. The rate of osteolysis in THRs is higher than in TKRs, which may be attributed to volume and size of UHMWPE wear particles, therefore; larger particles in TKR can induce less inflammatory macrophages [29].

2.3 *In vivo* Wear Rate of Total Knee Replacement

Evaluation of *in vitro* and *in vivo* wear properties of UHMWPE tibial inserts is critical to improve the implant design, manufacturing process and also the material [2,32,33]. In vitro wear rates using simulators need to be validated in order to provide accurate wear rates [34]; therefore wear assessment of retrievals is necessary to provide more information about the performance of the UHMWPE tibial inserts. *In vivo* wear assessment has been done by numerous techniques such as semi-quantitative method to score damage modes [14], quantitative methods [8,9,35–38] to evaluate the worn areas, and also geometric analysis [11,33,39] to quantify the linear penetration and volumetric wear rate.

2.5 Wear Mechanisms

In biomedical devices such as a knee replacement, one or more wear mechanisms can be active. The four major mechanisms of wear are adhesion, abrasion, fatigue and tribochemical reactions (figure 2.2) [29,31,40–42]. Adhesion depends on various factors, such as mechanical properties, chemical properties and etc., of the contact surfaces. This mechanism usually occurs due to the bonding of two smooth surfaces pressed together under load and relative motion causing large plastic deformation in the contact region; therefore a crack can be initiated and reaches to the surface of the component. In this case, the material can come off from one or more surfaces usually from the weaker one, and generate the wear debris. In the case of a knee prosthesis, which contains metallic and polymeric parts, the latter material is the one that usually generates wear particles. Abrasion occurs when surface asperities of one surface penetrate a counter surface. This can lead to cutting, scratching and plowing (two-body wear). Additional abrasion can take place if hard particles enter the tribological interface (three-body wear). The most common wear mechanism in total knee replacement is surface fatigue, which is the result of repetitive rolling and sliding cycles that cause local stresses to exceed the fatigue strength of the material and induce surface or subsurface cracks. Under repeated sliding motion, the crack can grow and the contact region can be fractured and generate wear particles [31,41,42]. The tribochemical reactions can affect the chemical properties of surfaces and may prevent adhesion, therefore; tribochemical reactions can be beneficial on the wear behavior such as metal on metal implant. In this case the tribochemical reaction layers can be generated in the contact area and act as a solid lubricant and consequently reduce the surface fatigue [31]. This influence is not described yet for polyethylene components. Also the consequences of this phenomenon on the wear mechanisms is not yet investigated [31].

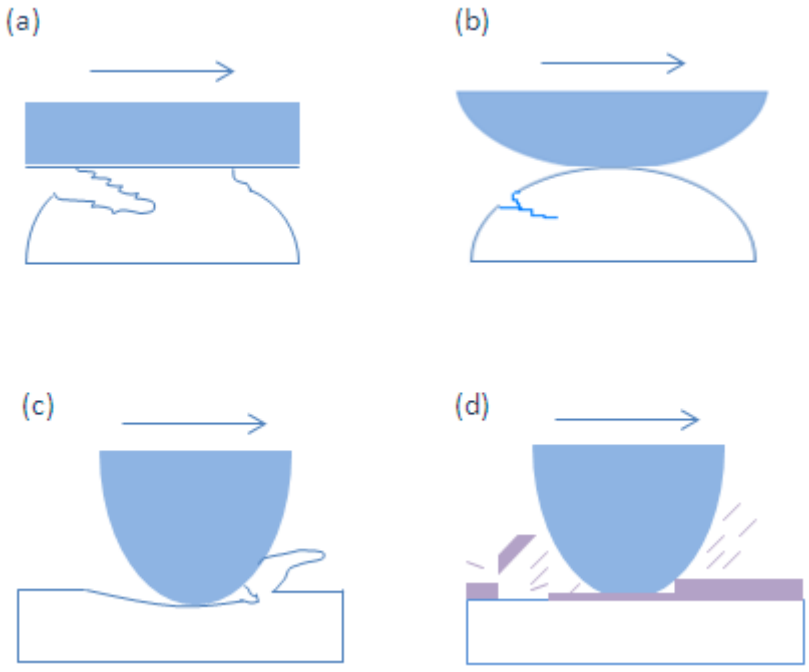

Figure 2.2 Schematic illustration of wear mechanisms (a) Adhesion, (b) Surface Fatigue, (c) Abrasion and (d) Tribochemical reaction [42].

2.4 Wear Features

Quantifying the surface damage in tibial inserts is critical to improve the implant designs. The visible damage of a surface due to wear is described as a wear appearance or wear features. polishing, burnishing, scratching, pitting, delamination, striation, abrasion, embedded debris and surface deformation are typical wear features on polyethylene tibial inserts (figure 2.3) [14,41].

The burnished feature which is characterized as wear polishing usually occurs due to the adhesion wear mechanism that tears and pulls off fibrils that initiated in the polymeric material during the sliding of the femoral condoyle on the tibial insert. Scratches have linear features on the articulating surface due to the presence of third-body particles in an abrasive wear mode. Pitting is a common wear feature characterized by mostly rounded small pits (<1 mm). Such pits

can be either caused by local surface fatigue or three-body wear (indentations by cement particles). Delamination is the most extreme wear feature and frequently occurred in early tibial insert designs, where the PE was sterilized in air. Increasing the degree of oxidation results in brittle material and leads to crack propagation underneath the articulating surfaces [40].

Striated pattern is a frequent wear pattern that usually occurs early after implantation on the UHMWPE surfaces of the retrieved inserts, due to the little knowledge about these patterns, it is critical to analyze the structure of the single striations which may causes of severe damage of the tibial inserts [16]. In the next section the striated pattern is described in detail . Abrasion is a rough and tufted region that can be visualized on the articulating surface of the tibial inserts. Embedded debris is another damage mode that can be observed as a different color or texture of particles embedded in the polyethylene insert articulating surface [38]. Cyclic deformation which is referred to as creep is a permanent change of the surface geometry such as form and dimension as well as molecular orientation in inserts. This type of damage does not correspond to wear since no particles are produced [40].

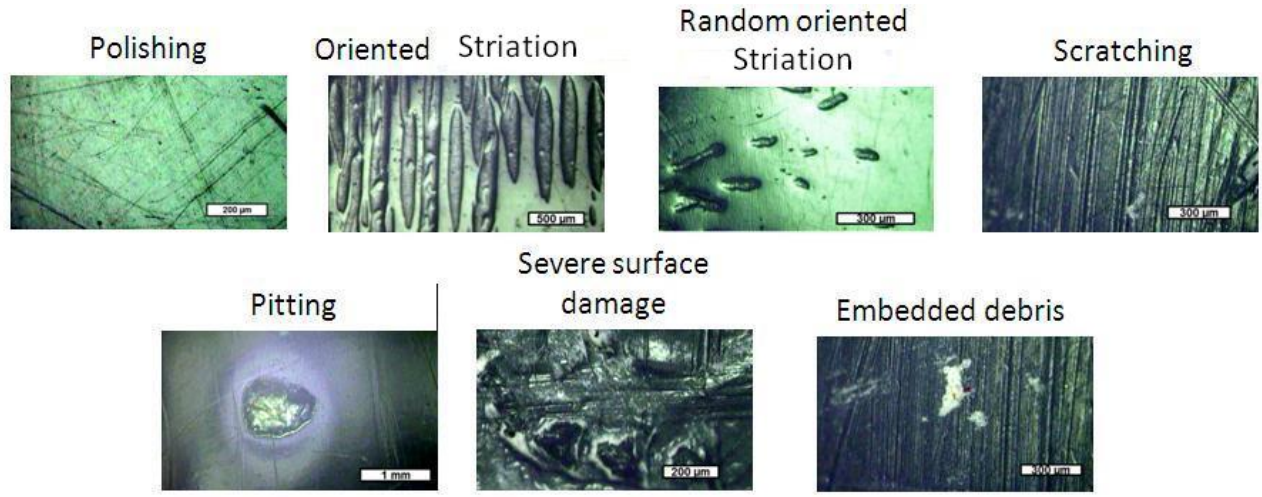

Figure 2.3 Different wear patterns.

2.4.1 Striated Pattern

Striated patterns can be observed on tibial insert surfaces relatively early after implantation. Contact mechanics of the knee can be responsible for the generation of the specific appearance of a striated pattern; therefore, analyzing striations can be helpful to understand the local kinematics of the tibial articulation and the reasons for severe damage of the articulating surface of tibial inserts. In contrast, the striated pattern has not seen replicated in the knee simulator under ISO conditions suggest that *in vivo* contact mechanics might be different [15].

The following three categories of striated patterns were observed on NexGen (Zimmer Inc.) tibial inserts: (1) An elongated striated pattern which is oriented in a single direction and the length to width ratio is greater than 6, (2) A short striated pattern with a length to width ratio less than 6, and the angle between the striations is less than 30°, and (3) A randomly oriented pattern with an angle of more than 30° between two neighboring striations. Figure 2.4 represents the three categories of striated patterns [21]. According to a Transmission Electron Microscopy (TEM) study of Wimmer et al.[15], the striations could be highly oriented polyethylene fibrils which align the antero-posteriorly in the same direction of the striation. The width of a single striation is about 70 μm and the darker elevations separated from the brighter regions, which are the valleys in-between.

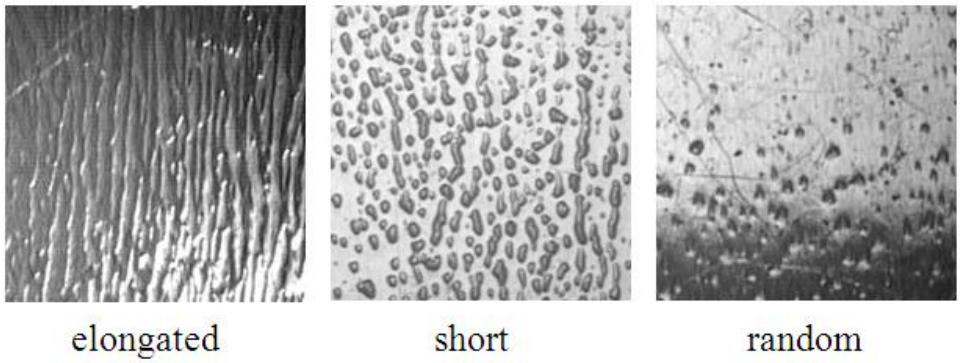

Figure 2.4 Three categories of striated patterns.

2.6 Deformation

The nonconformity of the articular surfaces between the tibial and femoral components causes a higher contact pressure due to the smaller contact area compared to the conforming contact conditions in a total hip replacement [2]. Therefore, the irrecoverable plastic deformation can be generated by reaching over the yield stress during the cyclic physiological loading of daily activities [40]. This phenomenon can affect the kinematic and tribological behavior of the knee joint. It has been shown that molecular rearrangement close to the surface in UHMWPE can be created during sliding. In the amorphous region, interlamellar shearing, interlamellar stretching and lamella rotation are the common mechanisms [40]. To deform the amorphous phase in polyethylene only 2-10% of activation energy of the chain-dislocation-slip in the crystals is needed and this deformation can be reversible up to the strain of 0.4% [40]. At higher strain, microvoids can be created in the amorphous phase and sufficient tensile load can cause a crack in the polymer. If higher strain occurs, the crystalline phase can be affected as well. During uni-directional loading the compression load causes a reorientation and rearrangement of crystals. In the multi-directional loading system, the role of tensile stresses is dominant in generating crazes and subsequent wear particles [40,43]. Various factors such as the amount of constraint, extend of oxidation in polyethylene, etc. contributing the wear rate affect the accuracy of the simulating the clinical performance of different design and material [2].

2.7 Characterization Techniques and Instruments

2.7.1 Raman Spectroscopy

Raman spectroscopy is a powerful technique that provides information about the structure, vibrational modes and morphological changes in materials [44,45]. Raman spectroscopy is based on inelastic scattering of monochromatic light such as a laser by

interacting with the vibrational frequencies of molecules which cause an energy level shift up or down from the photons. Thus, the molecular bonds can be identified, which provide the fingerprint for a specific chemical composition [46]. This technique is widely used for investigation the crystallinity, chemical and structural degradation of polyethylene by the correlation of the intensity of the vibrational bands [22,47–56]. The crystallinity of polyethylene can be determined from the vibrational bands within the wave-number region of 1500-900 cm^{-1}. This region can be divided into three regions as shown in Table I, region I is related to the carbon-carbon (C-C) stretching vibrational mode that is in the spectrum range of 1000-1150 cm^{-1} [40,57]. Region II is dominated by CH_2 twisting vibration around the Raman band of 1300 cm^{-1} [40,57]. Region III is for CH_2 bending in the range of 1350-1500 cm^{-1} [40,57]. Figure 2.5 shows a typical Raman band spectrum of UHMWPE.

Table I. RAMAN BANDS AND THE VIBRATIONAL MODES OF POLYETHYLENE [40,57]

Wave Number (cm^{-1})	**Mode**	**Phase**
Region I		
1060	ν_{as}CC (antisymmetric stretching)	Crystalline+ trans
1080	νCC (stretching)	Amorphous
1127	ν_sCC (symmetric stretching)	Crystalline+ trans
Region II		
1293	τCH_2 (twisting)	Crystalline
1305	τCH_2 (twisting)	Amorphous
Region III		
1414	δCH_2 (bending)	Crystalline
1440	δCH_2 (bending)	Crystalline+ trans
1460	δCH_2 (bending)	Amorphous

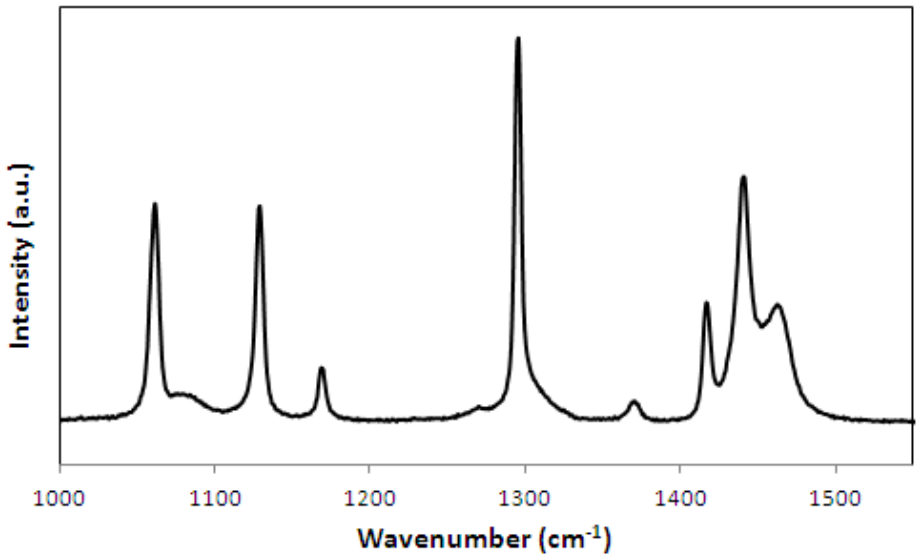

Figure 2.5 Typical Raman spectrum of UHMWPE.

The integrated intensity of the 1416 cm^{-1} which relates to CH_2 bending vibration (region III) can be used to measure the relative amount of CH_2 units in the crystal phase of UHMWPE. Specifically it represents the orthorhombic lattice which can participate in the scattering at this frequency [58]. The twisting region (region II) is independent of chain conformation (crystalline and amorphous contents) and it calls internal intensity standard [59].

According to the Strobl and Hagedorn method [59], the relative content of three different interphases can be estimated. α_o, the fraction of orthorhombic crystalline phase (Eq. 2.1), α_a, the amorphous phase (Eq. 2.2) and α_b, the interphase (Eq. 2.3) (intermediate anisotropic disorder and the chains are stretched, but have lost their lateral order) can be calculated from the relative intensities of the specific Raman bands [44,48,59]:

$$\alpha_o = \frac{I_{1416}}{0.46 \times I_{1295+1305}} \quad (2.1)$$

$$\alpha_a = \frac{I_{1080}}{0.79 \times I_{1295+1305}} \quad (2.2)$$

$$\alpha_b = 1 - (\alpha_o + \alpha_a) \quad (2.3)$$

I_{1416} and I_{1080} are the integrated areas of the Raman bands at 1416 cm^{-1} (which assigned to CH_2 bending) and 1080 cm^{-1} (assigned to CC stretching) respectively. The Raman band at 1295 cm^{-1} which is situated around 1305 cm^{-1}, is assigned for the CH_2 twisting. $I_{1295+1305}$ is the area of the internal standard band group, since the spectra region between 1250-1350 cm^{-1} is independent of the polymer chain conformation [44].

In the equation 2.1, the constant 0.46 was determined from the spectra of 100% crystalline polyethylene. The amorphous phase content can be calculated from the integrated intensity of the 1303 cm^{-1} broad band in the twisting region. Also the amorphous content can be calculated from the 1080 cm^{-1} band in the stretching region. Since the deconvolution of the latter spectral region is more straightforward, equation (2.2) is mostly used to determine the amorphous content. The constant in the equation has been obtained from the spectrum of fully melted polyethylene [59].

The interfacial region in semicrystalline polymers is an extended, trans-configuration of the chains with no lateral order which is located between the crystalline and amorphous layers [58].

2.7.2 Infrared Spectroscopy

Infrared spectroscopy is one of the most common techniques to analyze solids, liquids or gaseous states and is commercially available since the 1940s. Similar to Raman spectroscopy,

Infrared spectroscopy is based on the vibration of atoms in the molecules by passing the infrared radiation through the sample and analyzing the amount of absorbed energy of the incident radiation. Therefore; each peak within the spectrum represents the absorbed energy due to the frequency of the vibration of a particular molecule [60]. Vibrational information of each covalent bond in a molecule can provide a fingerprint by which the molecule can be identified [61].

The Infrared spectrum is unique to a specific molecule and can be used to determine its structure and is usually plotted as the absorbance versus the wavenumber (number of waves in one centimeter of the path line and inversely proportional to the wavelength) [61].

2.7.2.1 Fourier Transform Infrared Spectroscopy

In Fourier transform Infrared spectroscopy (FTIR) the interferometer which consists of an Infrared source, beam splitter, mirror, laser and detector, measures the spectrum. By processing the data of the recorded signals (interferogram) through the Fourier transform technique the sample's spectrum can be built [54].

Two different types of FTIR are: (1) Transmission FTIR and (2) ATR-FTIR (Attenuated Total Reflectance FTIR).

1) Transmission FTIR: Here, the Infrared radiation passes through the sample and the transmitted energy is measured and the spectrum can be generated. In transmission FTIR, the thickness and the orientation of the sample to the directional plane of the beam are determined as the effective path length in the sample. To prevent totally absorbing bands, the sample should be transparent and available as a thin film [61].

2) ATR-FTIR: The infrared beam reflects internally from the crystal to the sample at a specific angle and creates the evanescent wave in the sample. Some of the

energy absorbed by the sample and the evanescent wave will be attenuated and returned to the crystal. It exits from the opposite end of the crystal where it is picked up by the detector (figure 2.6) [61]. In contrast to the transmission FTIR, there is minimal or no sample preparation needed [62]. Zinc Selenide (ZnSe) and Germanium(Ge) are the most commonly ATR crystals [63].

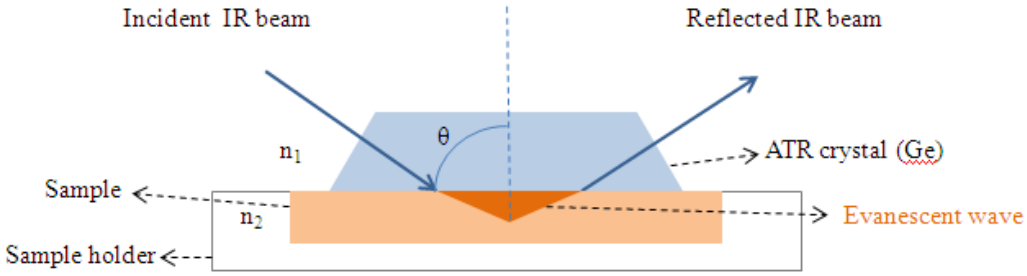

Figure 2.6 Schematic of typical ATR-FTIR cell [63].

The depth of penetration of the IR radiation in the sample depends on the wavelength (λ), angle of incident radiation (θ) and refractive index of crystal (n_2). In the following equation, the depth of penetration function in a non absorbing medium is shown [61]:

$$d_p = (\lambda/n_1)/\{2\pi[sin\theta - (n_1/n_2)^2]^{1/2}\} \qquad (2.4)$$

n_1 is the refractive index of the sample.

Main absorption of polyethylene in the IR region and their assignments is shown in the table II.

Table II. MAIN ABSORPTION BANDS AND THEIR ASSIGNMENT OF POLYETHYLENE IN IR REGION [64–66]

Band (cm^{-1})	**Assignment**	**Intensity**
2914	CH_2 asymmetric stretching	Strong
2842	CH_2 symmetric stretching	Strong
1472	CH_2 bending (crystalline)	Strong
1462	CH_2 bending (amorphous)	Strong
1377	CH_3 symmetric bending	Weak
1366	CH_2 wagging	Medium
1351	CH_2 wagging (amorphous)	Medium
1306	CH_2 twisting (amorphous)	Weak
730	CH_2 rocking (crystalline)	Medium
720	CH_2 rocking (amorphous)	Medium

Infrared spectra method is widely used to characterize the semi-crystalline polymers due to the fact that this method is sensitive to the conformation of the molecules and the packing of their chains [67]. Typical polyethylene absorptions at 720, 730, 1462, 1472, 2842 and 2914 cm^{-1} [68,69] are evident. Two regions of 715-735 and 1420-1475 cm^{-1} which relates to methylene rocking and scissoring mode, respectively, were widely used to determine the crystallinity of polyethylene [69–72]. In the first region, from the three rocking mode bands, two (720 and 730 cm^{-1}) are related to the crystalline phase with narrower bands compare to the amorphous phase near 720 cm^{-1} which lies hidden under the two narrow bands [69]. The second region which relates to the methylene scissoring mode is very similar to the first region. The two bands at 1462 and 1472 cm^{-1} are related to the crystalline phase and a broader band near the 1462 cm^{-1} is considered as an amorphous band, which is also hidden under the two other bands [69].

According to the Zerbi et al [70] the percentage of the crystalline content, X_c, can be calculated using equation 2.5 [70]:

$$X_c = 100 - \frac{1-\left(\frac{I_a/I_b}{1.233}\right)}{1+(I_a/I_b)}.100 \qquad (2.5)$$

In this equation, I_a and I_b are the absorption intensities corresponding to the bands of 730 and 720 cm^{-1} or, the bands 1462 and 1472 cm^{-1} as well [70]. The constant 1.233 has been verified experimentally and corresponds the relation of intensities of these bands for totally crystalline high density molecular weight polyethylene [70]. The amorphous band in the region of 1420-1475 cm^{-1} is highly asymmetric which makes the band fitting more difficult and less accurate compare to the first region (715-735 cm^{-1}) [69,70,73], therefore; in this study the rocking mode bands at 715-735 cm^{-1} are used.

Chapter 3. Materials and Methods

3.1 Wear Assessment of Retrieved Tibial Inserts

The complex geometry of contemporary tibial inserts poses a challenge for precise radiographic wear assessment leading to inaccurate linear wear measurements [8,9]. In addition, it is not clear how maximum linear penetration translates into volumetric wear loss and particle burden. The purpose of this study is to retrospectively determine the linear wear penetration and the volumetric wear of tibial inserts retrieved after revision surgery or postmortem. The first hypothesis of specific aim 1 is that maximum linear penetration can serve as a good surrogate for volumetric wear loss.

3.1.1 Sample Groups

Polyethylene wear was assessed for retrieved tibial inserts of a single cruciate retaining TKR design (NexGen CR, Zimmer Inc., Warsaw, IN). The retrievals were collected at Rush University Medical Center throughout the years of 2000 to 2012. In figure 3.1, a surgically retrieved tibial insert used in this study is shown. The steady-state condition in retrieved tibial inserts usually achieved after 1 year time *in situ*. In case of revision retrieved inserts there are relatively large number of implants that failed due to infection or other non-wear related complication within the first two years. Often these insert show little wear. Therefore; revision retrievals were only included if they were implanted for longer than two years. All postmortem retrievals except of one were implanted for more than two years. Postmortem retrievals were considered as well-functioning components because no failure of the implant had occurred. Therefore, all components with a time *in situ* of more than 1 year were considered. This inclusion criteria resulted in a group of 85 retrievals, however four inserts had to be excluded due to excessive wear and surface deformation that made the mathematical reconstruction of the

surface and therefore accurate wear assessment impossible. Thus, there was a final group of 81 retrievals with an average time *in situ* of 5.27±2.89 years. Within this group 14 tibial inserts were retrieved postmortem and the remaining implants were retrieved upon revision surgery. The time *in situ* ranged from 1.58 to 15.58 years and from 2 to 12.78 years for the postmortem group and the revision group, respectively. The tibial inserts were made from conventional UHMWPE compression molded and gamma sterilized in nitrogen. There were four different component sizes included in the retrieval group which were labeled by the manufacturer, from the smallest to the largest, as purple, yellow, green and blue. Dimensions for width and length are given in Table III. There were a total of 1 purple, 45 yellow, 27 green and 8 blue. Also, the components had various nominal thicknesses ranging from 10 to 20 mm.

Figure 3.1 UHMWPE NexGen cruciate-retaining tibial insert.

Table III. DIMENSION OF AVAILABLE RETRIEVED TIBIAL INSERTS

Size	**Width [mm]**	**Length [mm]**
Purple	36.2	56.1
Yellow	37.8	63.6
Green	43.0	72.7
Blue	45.8	79.5

Reasons for revision included aseptic loosening (27%), infection (20%), instability (11%), pain (11%) and stiffness (4%). For some patients there was more than one failure reason listed. For 27% of patients the reason for revision was unknown. The reasons of revision due to failure are plotted in figure 3.2.

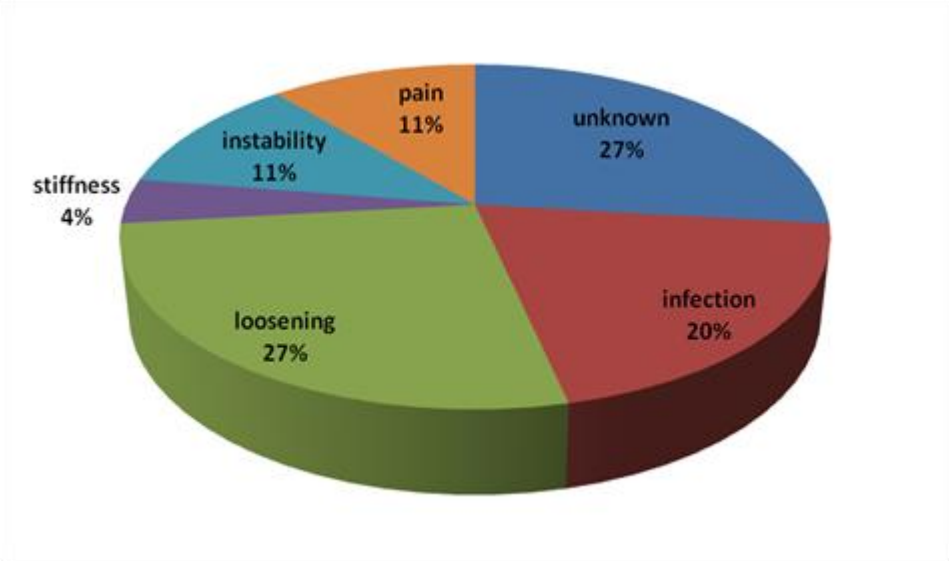

Figure 3.2 Failure reasons for revision retrieved tibial insert.

The overall average patient age at implantation was 63.32±11.00 years (range: 37-88 year). There were 20 male and 60 female patients, and 1 unknown. In 34 cases the left-side and in 47 cases the right-side was affected. There were 3 bilateral cases. The demographics of these two groups are summarized in table IV (adopted from [74]).

Table IV. PATIENT DEMOGRAPHICS FOR RETRIEVED IMPLANTS

Implant design	**Number of explants**	**Patient age at surgery (years)**	**Implantation time (years)**	**Sex(male/ female/un known)**	**Side(left/ right)**	**Component thickness (mm)**	**Cemented femoral and/or tibial component**	**Material of femoral component**
CR NexGen	81	63.3 ± 11.0 (37-88)	5.2 ± 2.9 (1.58-15.58)	20/60/1	34/47	12.0 ± 2.2 (10-17)	81/81	All Co-Cr-Mo

3.1.2 Optical Analysis

Prior to analysis all retrievals were cleaned with a standard cleaning protocol. This cleaning protocol entails several cleaning steps using water, enzymatic soap, 70% Isopropyl alcohol, and sonication. To visualize damage on the articulating surface of the tibial inserts optical analysis is needed.

3.1.2.1 Coordinate Measuring Machine (CMM)

The video and multi sensor metrology measuring system (SmartScope, OGP, Inc., Rochester, NY) was used to perform visual analysis on the retrieved tibial inserts. The SmartScope contains a xy stage and a vertically aligned optical lens system including a video capturing system. Therefore, the CMM has the ability to measure x, y, z coordinates of the tibial insert's location. Furthermore, a measuring routine can be generated using the MeasureMind software (OGP, Inc., Rochester, NY) to capture metrology data for all tibial inserts. Touch probe and laser sensors in a flash system enable the SmartScope to automatically conduct dimensional measurement of complex surfaces such as tibial inserts. To control the appearance of the image that is shown on the monitor, changing the focus, light level and magnification can provide a desired image. The light intensity can be adjusted for an optimal image. Back lighting is used to create a contour of a component by providing the light through the stage glass. For the three-dimensional images, ring light, which is located in the top can be used. The coaxial light can provide the illumination from the top to adjust a good contrast on flat surfaces. Figure 3.3 shows the coordinate measuring machine that was described earlier.

Figure 3.3 Coordinate measuring machine (SmartScope, OGP, Inc).

The outline of each tibial insert was mapped using the CMM (figure 3.4). First, the sample needed to be visually inspected for the presence of wear scars and different patterns. Then the surface was scanned with a laser to digitize the surface of the tibial inserts. The curvature of the articulating surface of NexGen tibial inserts makes optical evaluation with the optical capturing system of the CMM challenging. Therefore, it is important to visualize and draw the wear pattern of each component in the lab book to trace the wear scar easier with the CMM.

Unlike the MG II design, the NexGen tibial inserts articulating surface exhibits wear features such as scratching, pitting, creep, striation and polishing over large areas due to its higher conformity with the femoral component. For this study, there was a special focus on the

presence of so-called striated wear patterns which was reported by Wimmer et al [15]. Unlike previous studies, there was no distinguishing between different types of striated patterns (AP striations, ML striations and randomly oriented ones). Areas with striations were mapped on both the medial and lateral sides.

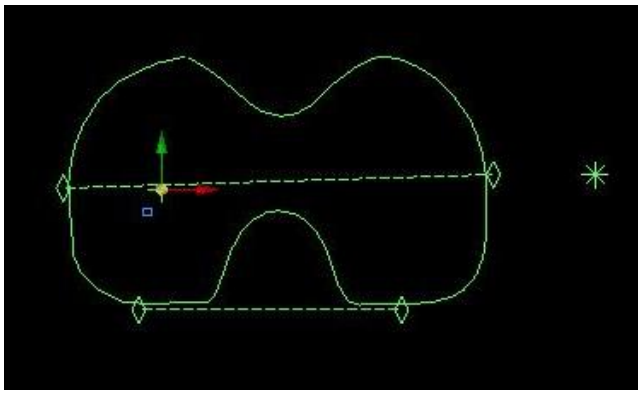

Figure 3.4 Typical NexGen tibial insert contour mapped by CMM.

To scan the surface of the tibial insert, the laser light can digitize the anterior-posterior line with spacing of 100*100 μm and depth accuracy of 2 μm. A total of 400,000 three-dimensional data points were gathered to reconstruct the articular surface of inserts utilizing a novel established autonomous mathematical reconstruction method [11]. The scanning time is dependent on the size of the tibial insert, ranging from 15 to 22 hours for the same accuracy (Figure 3.5).

Figure 3.5 Scanning the tibial insert articulating surface with SmartScope.

3.1.3 Autonomous Mathematical Reconstruction Method

There are various methods that researchers use to evaluate damage of the tibial inserts, such as semi-quantitative method to score the damage patterns [14], quantitative methods involving calculation of the wear areas [37,38], and also quantifying the linear penetration from patients' radiographs [8,9], or measuring with calipers [35,36] or dial indicators [35,75]. More recent methods, which provide the valuable information of the spatial distribution of the wear and deformation and consequently the amount of wear volume loss and maximum linear penetration, are CAD models or micro-CT [33,39]. Each method has several limitations to measure the volume loss of the articulating surface of tibial inserts accurately and efficiently. Recently, Knowlton et al. [11] created a novel method to calculate the volume loss from metrology data without knowledge of the original geometry of the surface which is an important factor since the information of the original surface is usually not available before implantation. One of the limitations of other methods to generate the spatial distribution of the surfaces is their low scanning resolution and consequently their accuracy, which is an issue to evaluate the low

rate volume. According to the Knowlton et al. [35] study, the autonomous mathematical reconstruction method is able to quantify the wear volume loss with small error of less than 5 mm^3 for each tibial plateau. In this method, the sample surface is fitted to unworn regions instead of polynomials or other curve fitting methods. Figure 3.6 illustrates the curve fitting of a design-congruent curve to the unworn points that adopted from [11]. However, as with all volume bases measurements, a limitation is that volume change due to wear and deformation are indistinguishable on the individual insert [11].

Figure 3.7 shows a reconstructed penetration map of a revision retrieved tibial insert, which was generated through the autonomous mathematical reconstruction method. As illustrated, the penetrated areas due to wear can be localized and quantified by using a custom written software (Matlab R2012a) code as described in [11]. The deeper linear penetration can be seen in the medial plateau and the value of the maximum linear penetration in the medial and lateral side is 0.52 and 0.25 mm, respectively.

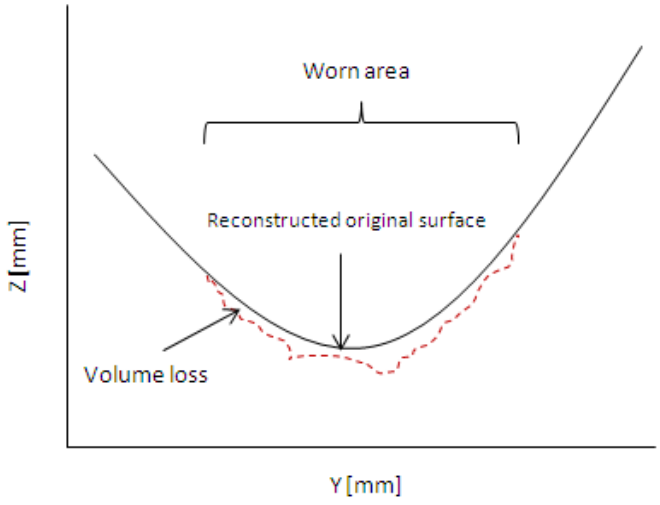

Figure 3.6 Autonomous mathematical reconstruction method fits a design-congruent curve to the unworn points to estimate the original surface (solid line) in a worn area (dashed line)[11].

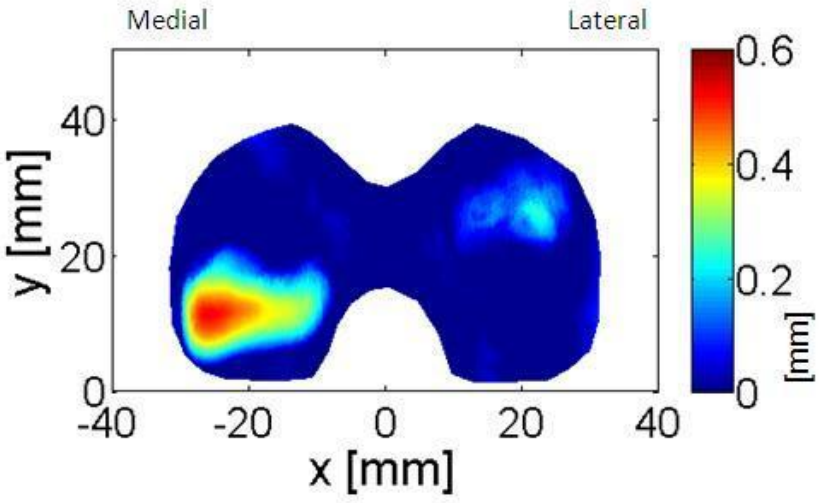

Figure 3.7 Penetration map of a tibial liner retrieved after 3.05 years in situ.

In this study, the worn areas of the tibial inserts often exhibited edge deformation and numerous pits. As mentioned in Chapter 2, deformation/creep is a permanent change in the surface geometry, additionally, this type of damage does not correspond to wear since no particles are produced [40]. Volume change due to edge deformation is not related to material loss and would therefore bias the assessment of the wear volume. Therefore, volume alteration due to edge loading was removed during the wear assessment process. The process of removing of the edge deformation artifact in one of the revision retrieved tibial insert is shown in figure 3.8.

As mentioned earlier, excessive pitting in conforming TKR designs is usually generated by three-body wear (usually bone cement particles) [17,74]. The process of pitting appears to be a trough indentation of third bodies (bone chips, bone cement, etc) in which the surface undergoes local deformation with little to no material loss. According to Knowlton et al. [16] pitting has little contribution to volume loss but it may affect the quantification of the maximum

linear penetration and need to be removed analogous to edge deformation. Figure 3.9 illustrates the removal of the pits in one of the revision retrieved tibial inserts. In this case, by considering 98% of the highest value of linear penetration, the correct value and location of the maximum linear penetration can be achieved. Also the wear volume loss can be quantified accurately.

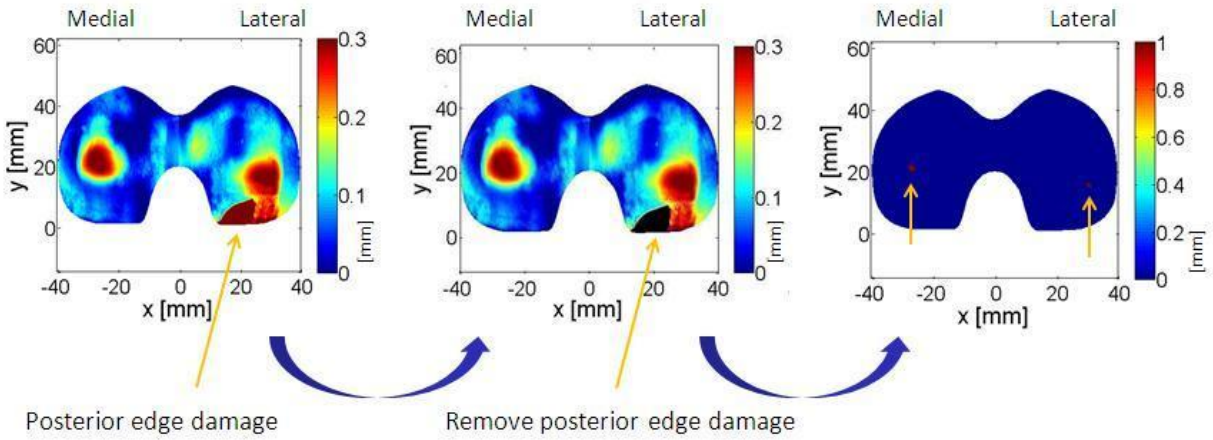

Figure 3.8 Process of removing edge deformation artifact.

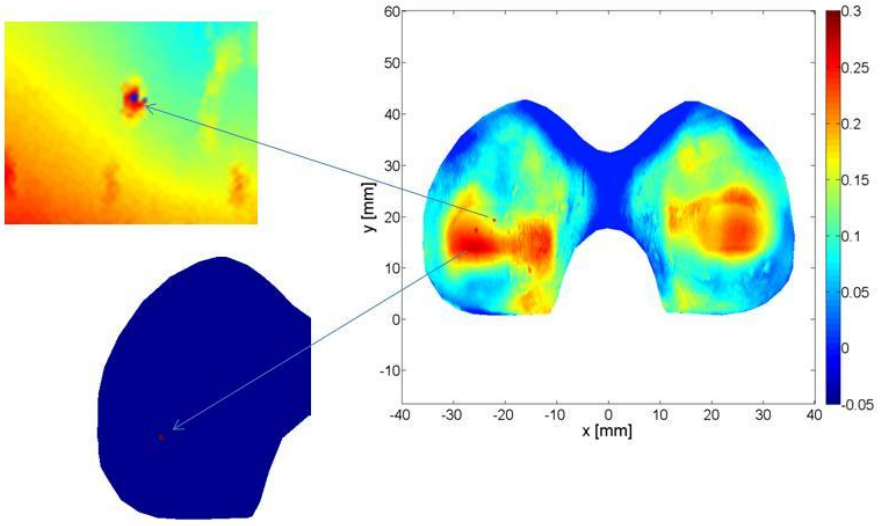

Figure 3.9 Process of removing the pit to localize area of the maximum linear penetration.

3.2 Impact of Patient Demographics on Wear Rate

The second hypothesis of the first aim in this study is that variables such as patient age, gender, height, weight BMI may have an impact on the wear behavior of a TKR tibial insert and thus implant survivorship. The age at the implantation surgery was available for all 81 patients. The gender of one patient was unknown; therefore the group of 80 was available for further analysis. Information of height and weight was available for a subgroup of 67 patients.

3.3 Striated Wear Pattern

Striated patterns could be observed in 61 out of 81 of the retrieved tibial inserts. To investigate if the presence of striated pattern can be an indicator for high wear, the areas exhibiting striated patterns on the medial and lateral side of the tibial insert were mapped with a CMM (SmartScope, OGP). Due to the variability of sizes of the retrieved tibial inserts, all outlines and mapped areas were normalized to a right component and dimensions corresponding to a nominal size (green) as defined by the manufacturer. In some tibial inserts there was more than one area of striations in each plateau, which were summed up to a total striated area. The values of the areas were numerically analyzed by the function of 'polyarea' in Matlab software. The striation area was calculated as a percentage of the total medial or lateral articular area.

3.4 Statistical Analysis

The relationship between wear (volumetric and penetration) and time *in situ* was determined by linear regression model. Volumetric wear and penetration rates were also compared by linear regression model. The impact of different patient factors on the volumetric wear rate was determined by Pearson Correlations. The impact of different factors (gender, age, weight, height) on the volumetric polyethylene wear rate was determined with a general linear model. Significance was set to $p=0.05$. Statistical analyses were performed in Excel (Microsoft

Corp, Redmond, CA, USA) and SPSS (SPSS Inc, Chicago, IL, USA). Reported data are displayed as mean ± SD unless noted otherwise.

3.4 Characterization of Striated Pattern Crystallinity

As mentioned earlier, understanding the morphology of the striated pattern can provide useful information about the *in vivo* contact mechanics and the conditions. To determine the crystallinity content of polymers, various methods such as Differential Scanning Calorimetry (DSC), Raman spectroscopy, Fourier Transform Infrared Spectroscopy (FTIR), etc. can be used. From literature it is not clear which method is more suitable for the determination of crystallinity in polyethylene [66,67], especially with regard to specific surface features instead of bulk material samples. Raman spectroscopy and FTIR with ATR attachment enable non-destructive analysis of surface features with a size of tens of micrometers. Therefore, both methods were used to investigate the crystallinity of samples.

3.4.1 Samples

In order to validate the method of crystallinity calculation by Raman spectroscopy and FTIR techniques, four control samples with known crystallinity were used. UHMWPE samples (control) with different crystallinity were supplied by Orthoplastic Ltd. (Lancashire, UK). Samples were taken from bar stock (10 ± 0.5 mm) that had been compression molded followed by various cooling methods (oven, air, liquid nitrogen, and water) to adjust different degrees of crystallinity. The crystallinity of each sample was measured by Orthoplastic by means of DSC (Table V).

Table V. NOMINAL CRYSTALLINITY OF UHMWPE SAMPLES PROVIDED BY ORTHOPLASTIC LTD.

Sample (UHMWPEs)	**Oven**	**Air**	**Liquid Nitrogen**	**Water**
% Crystallinity	53.98	51.91	48.85	47.91

In this study, to evaluate the structure of the striation, one representative tibial insert was chosen for analysis which exhibited a dominant presence of striations on both the medial and the lateral articulating surface. The *in situ* duration time for this component was 2.21 years.

3.4.2 Quantification of Polyethylene Crystallinity with Raman Spectroscopy

Raman spectroscopy has been largely used to identify marker bands of polyethylene and investigation the crystallinity, chemical and structural degradation of polyethylene by the correlation of their intensity of the bands [22,47–53,56].

3.4.2.1 Equipment

The Raman spectra in the 950-1600 cm^{-1} range were obtained using an Acton TriVista CRS Confocal Raman system with excitation radiation of an Ar-Kr 514.5 nm gas laser at ~10 mW with a microscope of 50X magnification and spectral resolution of 1.2 cm^{-1}. The spectra were obtained in a non-destructive way without any sample preparation. The Raman Spectroscopy apparatus was used by courtesy of department of Material Science and Engineering (Yifeng Liao, PhD) at Northwestern University (Evanston, IL).

For each control sample, five spectra were measured. Also, to analyze the striated pattern, five spectra were measured on the hill of a striation on the medial plateau and five on the lateral side of the retrieved tibial insert. The same number of spectra was measured within the troughs between two striations.

3.4.3 Quantification of Polyethylene Crystallinity with FTIR Spectroscopy

The IR spectra method is widely used to characterize semi-crystalline polymers due to the fact that this method is sensitive to the conformation of the molecules and the packing of their chains [15]. Therefore, to study the structure of the striated pattern FTIR spectroscopy was used.

3.4.3.1 Equipment

For the FTIR spectroscopy analysis a Bruker Tensor system (Hyperion 2000) was used by courtesy of Department of Civil and Environmental engineering and the Department of Earth and Planetary Sciences (Neil Blair, PhD) at Northwestern University (Evanston, IL). The device has the capability of transmission mode and Attenuated Total Reflectance (ATR) mode. To characterize the crystallinity of the UHMWPE the non-destructive FTIR-ATR method was used. The advantage of this method is that the spectra can be obtained directly from the surface without any further sample preparation. Also, it allows to optically targeting the sampling area.

For the ATR mode, the germanium crystal with an incident angle of 45° and 100 μm nominal diameter surface areas was used at 20X magnification and a spectral resolution of $4cm^{-1}$. The spectra were obtained with an accumulation of 32 scans in absorbance units from 600-4000 cm^{-1}. The effectiveness of the contact of the crystal with the sample surface will affect the quality of the obtained spectrum. There is a high interference due to moisture and carbon dioxide on the obtained spectra, therefore, the experiment has to be performed under vacuum. For each run, several minutes are required to achieve vacuum equilibrium.

To determine the band areas, in both methods, curve fitting analysis was performed in both regions using commercially available software (Origin 9.1). Curve fitting was performed on

the original spectra after baseline correction by using the linear combination of Gaussian and Lorentzian function (PsdVoigt1).

Chapter 4. Results

4.1 Wear Scar Area

Specific aim 1 was to determine the *in vivo* wear rate of a single cruciate retaining TKR design (NexGen CR, Zimmer Inc., Warsaw, IN). Therefore, the outline of the wear scar area was visualized and digitized by means of a coordinate measuring machine (SmartScope) for medial and lateral tibial plateau, separately. The wear scar area is a region, which, compared with newly manufactured components, underwent a morphological change at the surface, exhibiting wear patterns of pitting, scratching, polishing, burnishing and striation. To overlay the outline of wear scar areas for all 81 retrieved tibial inserts, the generated maps of different sizes were normalized to one common implant size ("green") for the right knee. The overlay of wear scar area demonstrates the frequency and location of the wear scar area on each tibial plateau for the entire sample group (figure 4.1). In figure 4.1, the increasing red-scale intensity (darker) indicates a higher frequency of inserts having damage in that specific location. This region was mostly located in the center and toward the outside edge of medial and lateral plateaus. According to the overlay plot, although the wear scar area (darker red scale) on the medial side larger than that of the lateral side, there is no significant difference between the wear scar areas on the medial and lateral tibial plateau ($p>0.05$, paired student t-test).

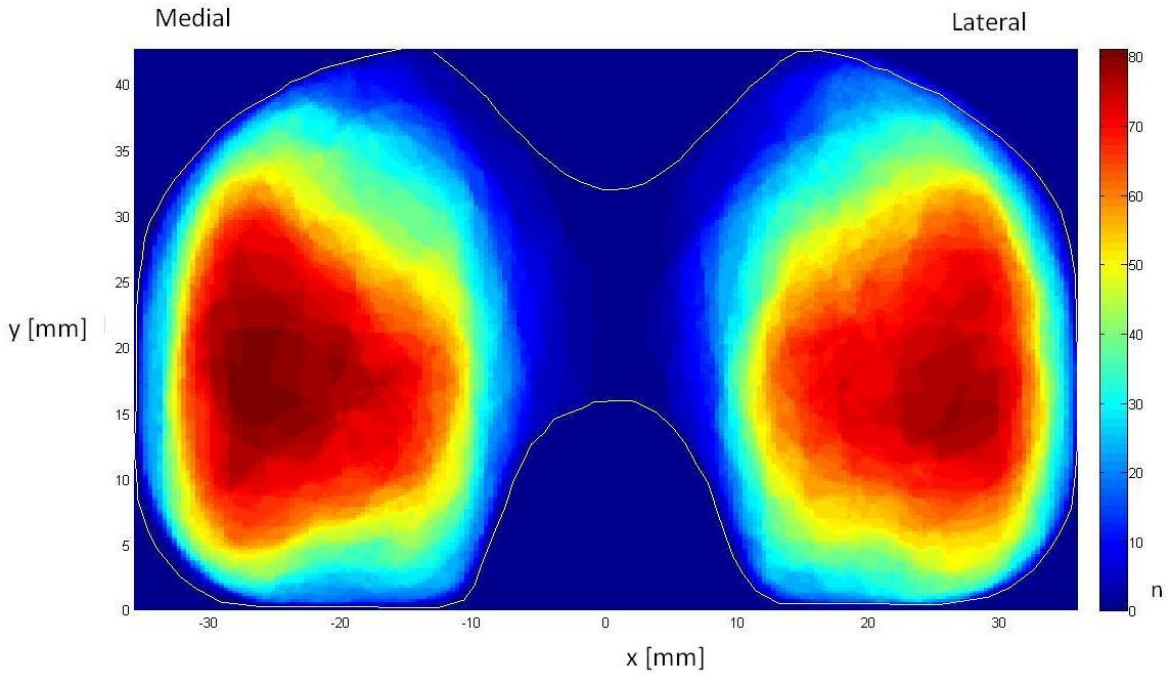

Figure 4.1 Overlay plot represents wear scar areas for all 81 retrieved inserts.

4.2 Aim1: Determine Accurate in vivo Wear Rate for Total Knee Replacement

4.2.1 Wear Volume Loss Assessment of Retrieved Tibial Insert

The average total rate of volume change for all 81 tibial inserts was 28.84±13.62 mm^3/year. In figure 4.2 the total volumetric change is plotted over time *in situ*. It can be seen that there is an intercept at 60.95 mm^3 and the slope is 13.81 mm^3/year. Considering the initial impact of creep during the wear process, it is appropriate to correct the volume change values by subtracting the intercept from each individual value. The resulting average wear rate of 13.98±11.7 mm^3/year is indicate to the slope in the regression model (13.82 mm^3/year, 9.74, 17.89, 95% CI, R^2=0.37, $p<0.001$). Between the lateral and medial compartments, the average rate of volume change was 15.60±9.96 and 13.23±6.44 mm^3/years, respectively. By considering the intercepts for lateral and medial compartments separately, the resulting values of the average

volumetric wear rate were 6.09±5.93 and 7.07±8.94 mm^3/years, respectively. These values are also in good agreement with the regression model for both the medial (6.9 mm^3/yr, 4.25, 9.55, 95% CI, R^2= 0.25, p<0.001,) and lateral sides (6.92 mm^3/yr, 4.7, 9.14, 95% CI, R^2=0.33, p<0.001) (figure 4.3). Comparison of wear rates for postmortem (22.65±8.73 mm^3/year) and revision surgery retrievals (30.55±13.88 mm^3/year) showed no significant difference (p= 0.143), therefore, all the retrieved tibial inserts were considered as one group.

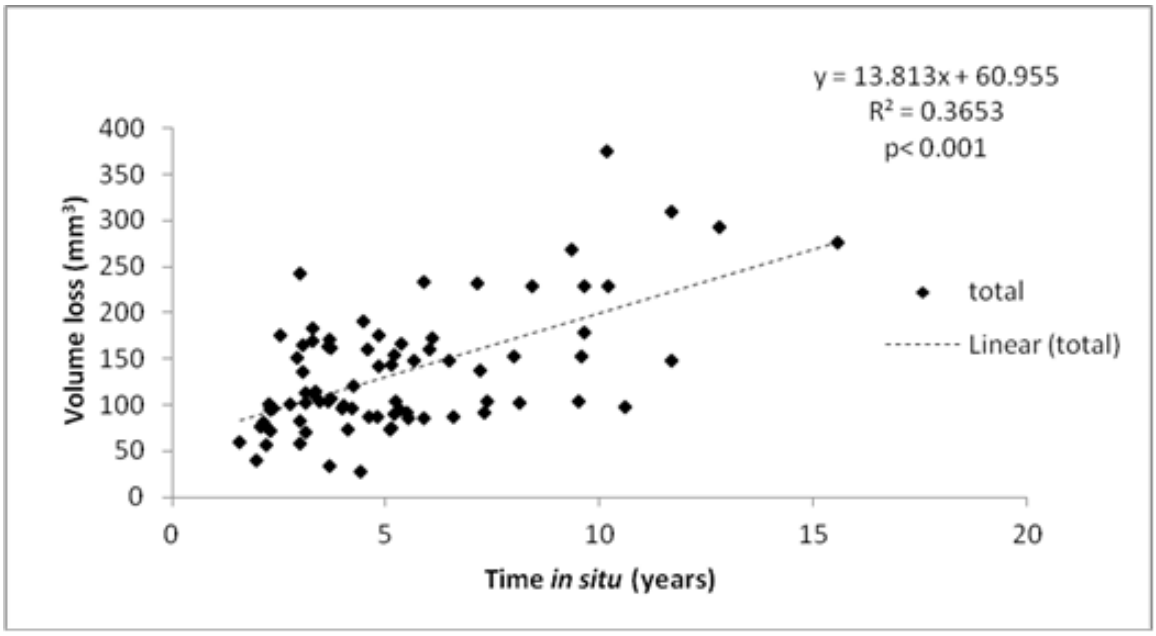

Figure 4.2 Total volume loss of articular surfaces for retrieved tibial inserts versus time in situ.

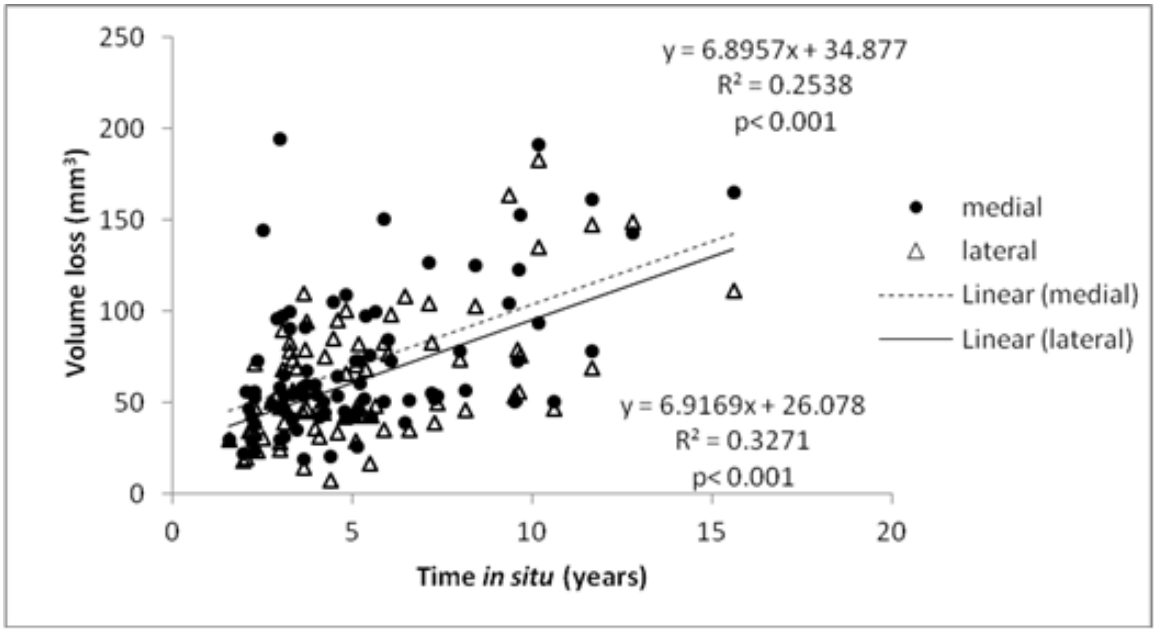

Figure 4.3 Volume loss of articular surfaces for medial and lateral retrieved tibial inserts versus time in situ.

4.2.2 Maximum Linear Penetration Measurement in Retrieved Tibial Insert

The maximum linear penetration of wear was calculated for medial and lateral side for each retrieved tibial insert. The average maximum penetration rate was 0.08±0.05 mm/year on the medial and 0.06±0.04 mm/year on the lateral side (Figure 4.4). After consideration of the intercept these values were corrected to 0.015±0.04 and 0.017±0.04 mm/year, respectively. There was only a weak linear association between penetration and time *in situ* on the medial (R^2=0.06, p=0.02) and lateral side (R^2=0.10, p=0.003).

Total maximum linear penetration, which is defined as the summation of the values for medial and lateral side, was 0.15±0.07 mm/year. The corrected value of the total maximum linear penetration for creep was 0.03±0.05 mm/year. There was a slightly better correlation between the total maximum linear penetration and time *in situ* (R^2=0.14, p<0.001) (figure 4.5), than their individual medial and lateral values.

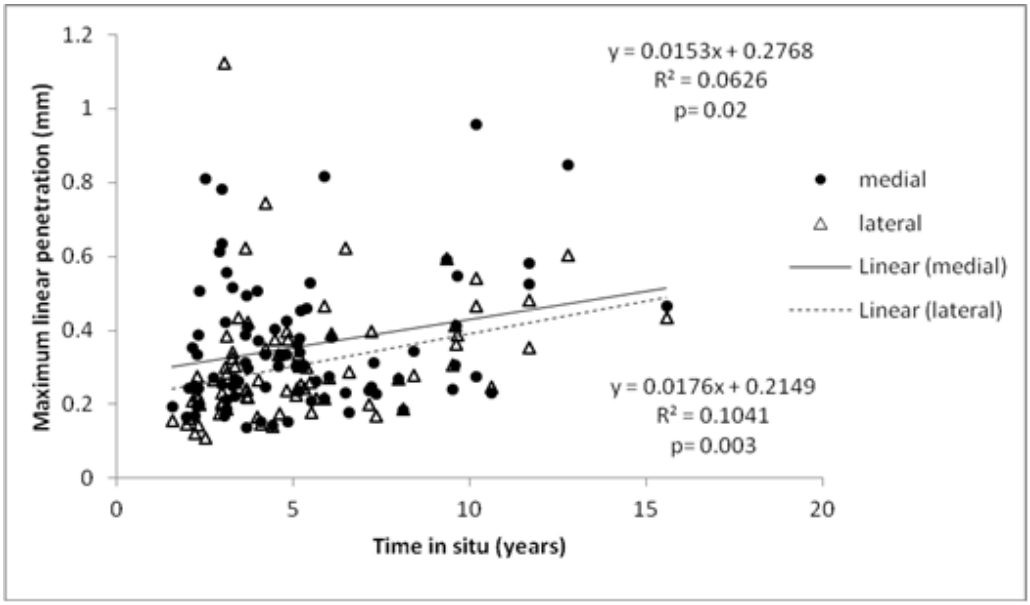

Figure 4.4 Maximum linear penetration of articular surfaces for retrieved tibial inserts versus time in situ for medial and lateral penetration.

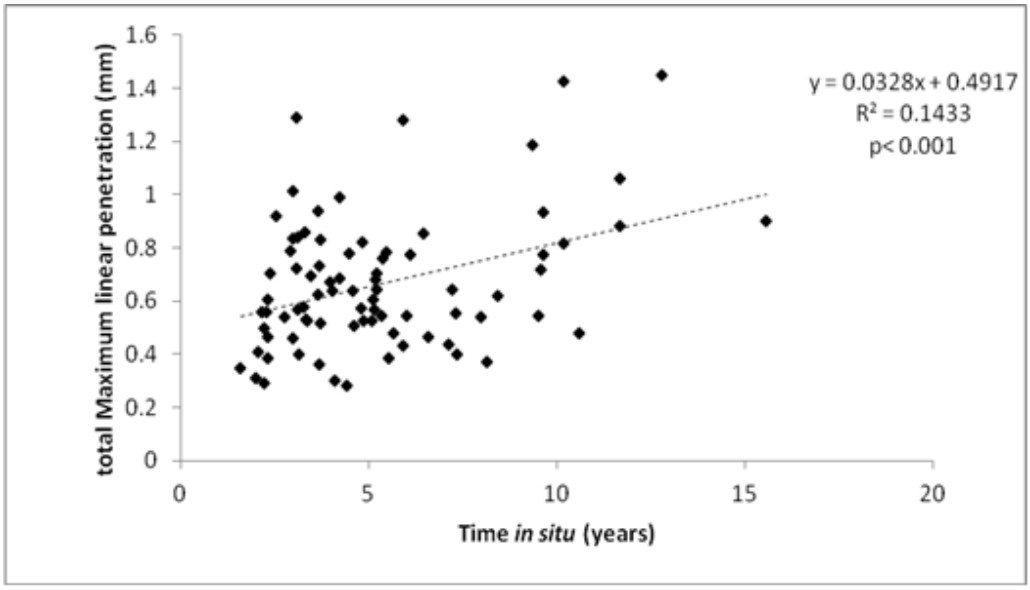

Figure 4.5 Maximum linear penetration of articular surfaces for retrieved tibial inserts versus time in situ for the total (medial side plus lateral side) penetration.

By separating the retrievals in two sub-groups of short term (between 2 to 5 year time *in situ*) and long term (>5 year time *in situ*), a linear regression model of the volume loss and time *in situ* shows that there is a better correlation for the long term retrievals. This may be explained by the effect of creep/deformation, which has an impact on the wear volume loss in the short time of the implant's life (R^2=0.07, p=0.07, R^2=0.38, p=0.007, for the short term and long term, respectively) (table V). For the two groups of revision and postmortem retrievals both had a good correlation between wear volume loss and time *in situ* (R^2=0.34, p<0.001, R^2=0.45, p=0.007, respectively).

Long term retrievals and postmortem retrievals have lower wear rates than their respective short term. The corrected wear volume loss is not significantly different in subgroups of short term and long term (p=0.274), or in revision and postmortem subgroups (p=0.143).

The maximum linear penetration rate on the medial and lateral sides is also higher for the short term retrievals compared to the long term ones which may be attributed to the creep effect in the short period of time *in situ*. Also, for the revision group, the maximum linear penetration rate values are higher in both medial and lateral sides compared to the postmortem ones, and the average time *in situ* in this group is almost half of the value for the postmortem group (p<0.001). Postmortem retrievals are considered as being well-functioning components, thus produces less wear/damage than retrievals [76].

Table VI. AVERAGE VALUES FOR TIME *IN SITU*, LINEAR REGRESSION OF VOLUME LOSS VS. TIME *IN SITU*, CORRECTED VOLUMETRIC WEAR RATE, MEDIAL AND LATERAL PENETRATION RATE FOR SUBGROUPS OF SHORT TERM, LONG TERM, REVISION AND POSTMORTEM RETRIEVED TIBIAL INSERTS.

	N	**time *in situ* [year]**	**linear regression: volume loss [mm^3] vs. time *in situ* [year]**		**corrected volume wear rate [mm^3/yr]**		**medial penetration rate [mm/yr]**		**lateral penetration rate [mm/yr]**	
		mean	slope	p-value	mean	p-value	mean	p-value	mean	p-value
all	81	5.2 ± 2.8	13.8	< 0.001	13.9 ± 11.7		0.08 ± 0.05		0.06 ± 0.04	
2-5 yrs *in situ*	45	3.3 ± 0.8	14.4	0.071	15.1 ± 14.0	0.274	0.11 ± 0.06	< 0.001	0.08 ± 0.05	< 0.001
> 5 yrs *in situ*	36	7.7 ± 2.6	18.1	< 0.001	12.4 ± 7.7		0.05 ± 0.02		0.04 ± 0.01	
revision surgery	67	4.6 ± 2.3	16	<0.001	14.6 ± 12.3	0.143	0.09 ± 0.05	< 0.001	0.07 ± 0.04	0.001
postmortem	14	8.4 ± 3.4	15.0	0.008	10.9 ± 7.3		0.04 ± 0.02		0.04 ± 0.02	

4.2.3 Comparison between Volumetric Wear, Penetration and Wear Scar Area

In order to determine whether penetration is a good surrogate measure for volumetric wear, the total of medial and lateral maximum penetration rates (0.15 ± 0.07 mm/year) were compared to the total volumetric wear rates (figure 4.6a). There was a good linear relationship (R^2=0.61, p<0.001). To investigate if the wear scar areas can be a good surrogate for volumetric wear; the volume loss rate is plotted versus the percentage of the wear scar area in the total area of the tibial insert (figure 4.6b). As can be seen, no correlation could be observed between the volume loss rate and the percentage of the wear scar area (R^2=0.008, p=0.49). Also, individual comparison on the medial and lateral sides showed similar trends for the correlation of the volume loss rate and maximum linear penetration (R^2=0.72, p<0.001, R^2=0.42, p<0.001, respectively) (figure 4.7a). For the wear scar area, the volume loss rate slightly correlated with the percentage of the wear scar area for the lateral tibial plateau (R^2=0.073, p=0.01) and for the medial side no correlation could be observed (R^2=0.0003, p=0.86) (figure 4.7b).

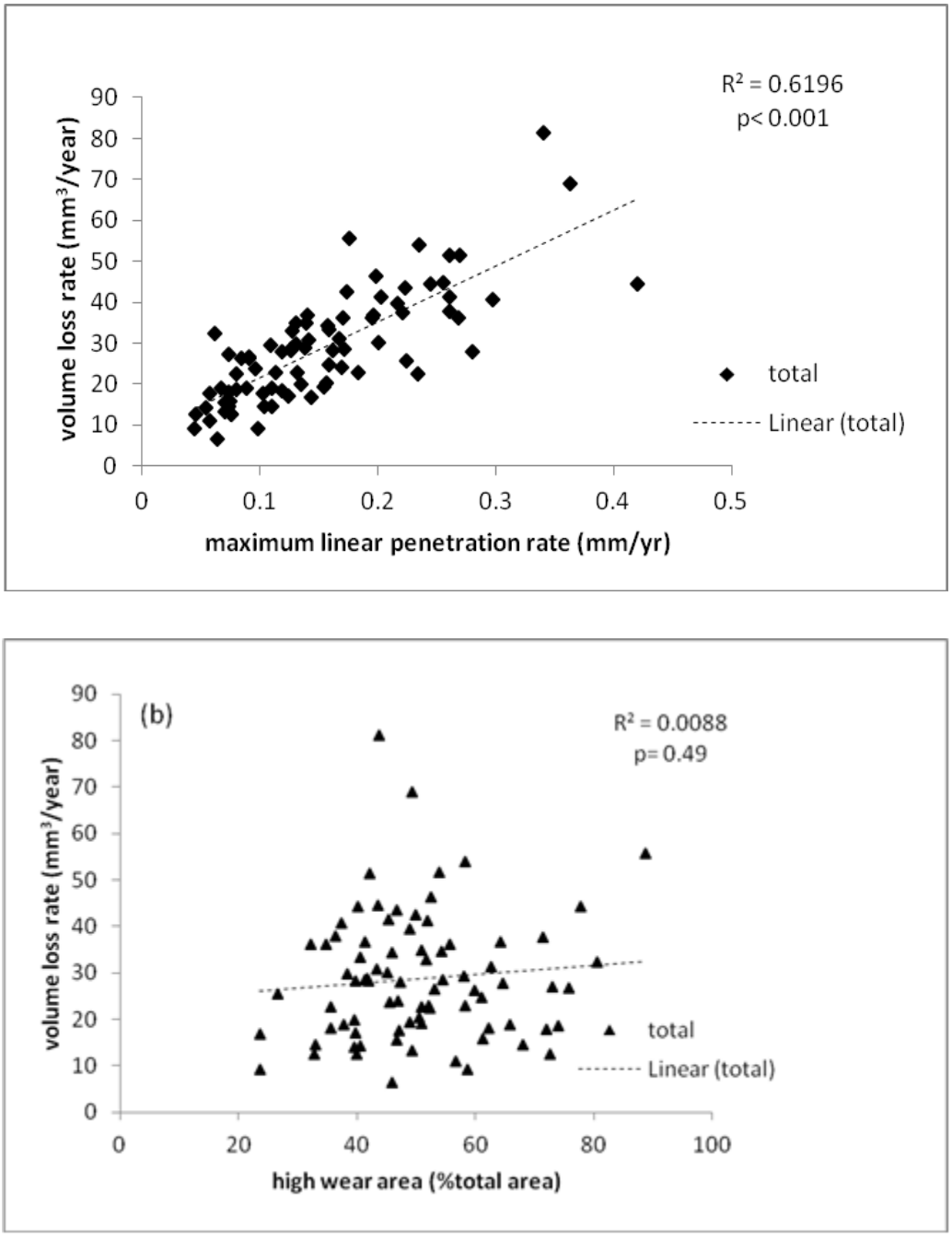

Figure 4.6 Correlation of total (medial side plus lateral side) volumetric wear rate to a) average maximum linear penetration rate and b) wear scar area (%total area) for 81 retrieved tibial inserts.

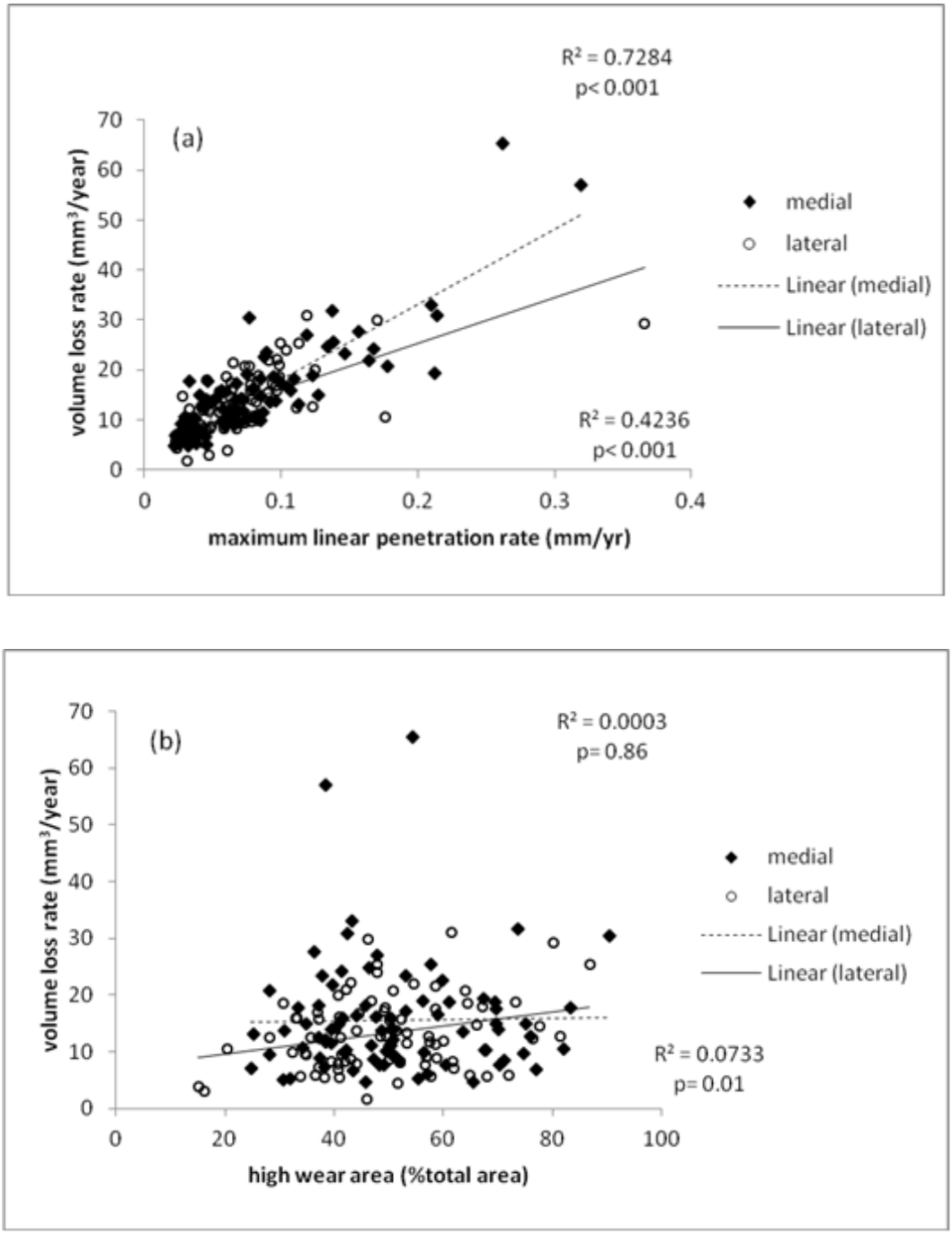

Figure 4.7 Correlation of medial and lateral tibial plateau of volumetric wear rate to a) average maximum linear penetration rate and b) wear scar area (%total area) for 81 retrieved tibial inserts.

By normalizing all the outlines of the retrieved tibial inserts, the most common location of the maximum linear penetration can be visualized. By considering 10% of the maximum value of the linear penetration for each retrieved tibial insert, the area can be quantified and localized for each component. Therefore, the overlay of these areas for all retrieved tibial inserts can be helpful to investigate where the most possible location of linear penetration is located.

The overlay of the areas for 10% of the maximum value of the linear penetration for the total of 81 retrieved tibial inserts for the medial and lateral side is illustrated in figure 4.8. Increasing the red scale intensity (darker) indicates more inserts that had higher linear penetration in a given location. The maximum linear penetration as displayed by the plot is mostly located posteriorly and with a tendency towards the outer edges. The location of the maximum linear penetration is spread out more on the lateral side than the medial plateau. The highest frequency of the overlaid areas is 12 and 19 on the lateral and medial plateau, respectively.

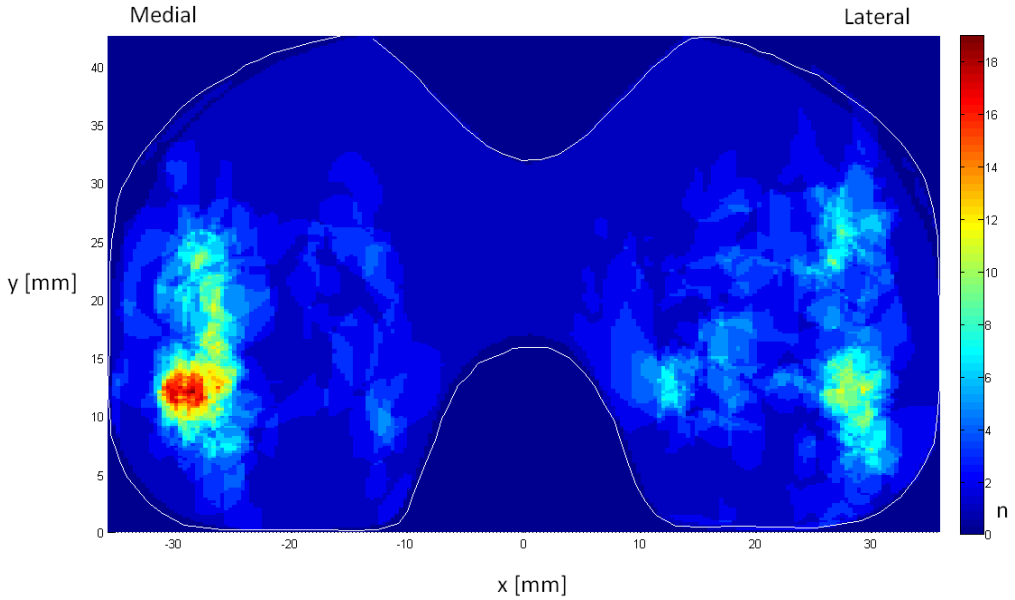

Figure 4.8 Overlay plot shows the location of 10% maximum value of the linear penetration for all 81 retrieved inserts.

Areal thickness changes (centroid of the 10% maximum value) were mapped for the lateral and medial sides with the help of an autonomous mathematical reconstruction method (figure 4.9). The minimum thicknesses of the four unworn reference components were used to compare with the areal thickness changes for all 81 retrieved tibial inserts (normalized: right side, size green). As shown in the plot, the thinnest part for each four references is located centrally for both medial and lateral sides. However, the minimum thicknesses of retrievals were spread out and mostly located posteriorly and toward the outside edges for both tibial compartments and also more spread out in the medial-lateral direction on the lateral side.

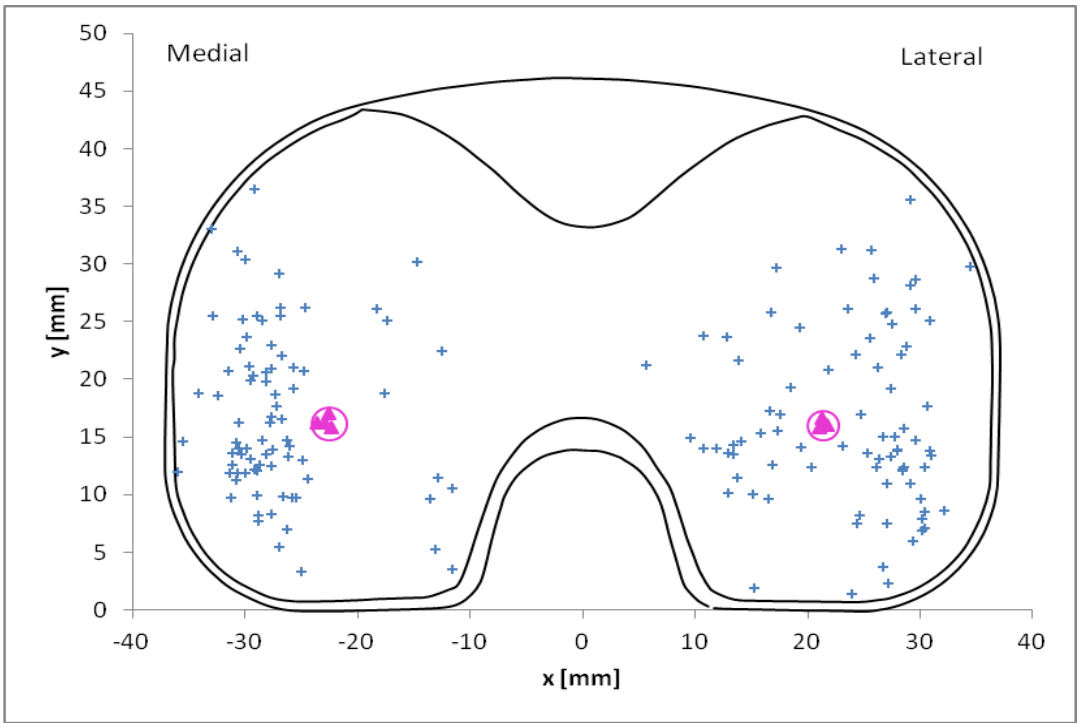

Figure 4.9 Location of thickness minimum identified with autonomous mathematical reconstruction showing retrievals (blue marks) and unworn reference components (pink triangles)

To investigate if the implant size could have an impact on the wear rate, the corrected volumetric wear rate was plotted versus the implant size (figure 4.10). By comparing the corrected wear rate in four implant sizes by means of a Krsukal-Wallis test, there was no significant difference found between them ($p>0.05$). Actually the median volumetric wear rates were very similar. Therefore, in this study the implant size was not considered as a significant impact factor for the wear rate.

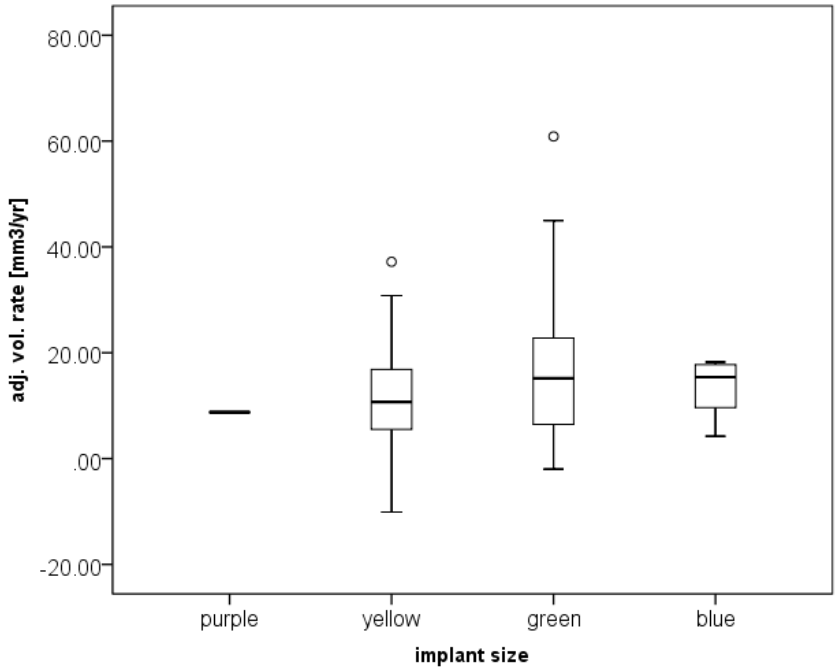

Figure 4.10 Box plot of corrected wear volume rate vs. implant size.

4.2.4 Impact of Patient Demographics on Wear

In regards to factors that impact the amount of polyethylene wear, it is well established that the activity level of the patient as well as the weight/BMI are determining factors. Generally younger patients are more active than older patients [12,77] and male patients are, on average, heavier than female patients. There is also an inverse relation between activity and obesity.

However, due to a lack of reference of *in vivo* wear rates, the exact relationship is not well established.

The impacts of age, gender and weight/BMI on volumetric wear rate were first tested with Pearson correlations. As mentioned in chapter 3, there was a case of unknown patient gender; additionally only the weight/BMI information was available for 67 out of 81 of the patients. Most significant factors were age and weight/BMI. First, an analysis of covariance was conducted to determine the impact of age and gender on the volumetric wear rate. Both factors were available for 80 of the 81 patients. These factors (age and gender), were shown to have a significant impact (p=0.002 and p=0.022, respectively), where lower age correlated to a higher wear rate and the female gender was related to a lower wear rate in the model. In figure 4.11 the total volume loss rate is plotted over the age for all 81 patients. As illustrated in the plot, there was a fair linear relationship between the total volume loss rate and age (R^2=0.11, p=0.002). By including BMI as an additional input factor the subject group was reduced to 67. In that case, age and gender remained significant factors (p=0.044, p=0.021), but BMI was not (p=0.094). By including weight instead of BMI in the model, weight remained as the only significant factor (p=0.044), whereas age and gender were no longer part of the model (p=0.134, p=0.087). Both BMI and weight correlated with a higher wear rate. For the subgroup of 67 patients the correlation of total volume loss rate versus weight and BMI are shown in figure 4.12 and 4.13, respectively. For this subgroup, there was a good correlation between the total volume loss rate and weight of the patients (R^2=0.17, p=0.001). However, the total volume loss rate increased slightly with the BMI, there is no significant correlation (R^2=0.03, p=0.13) (figure 4.13).

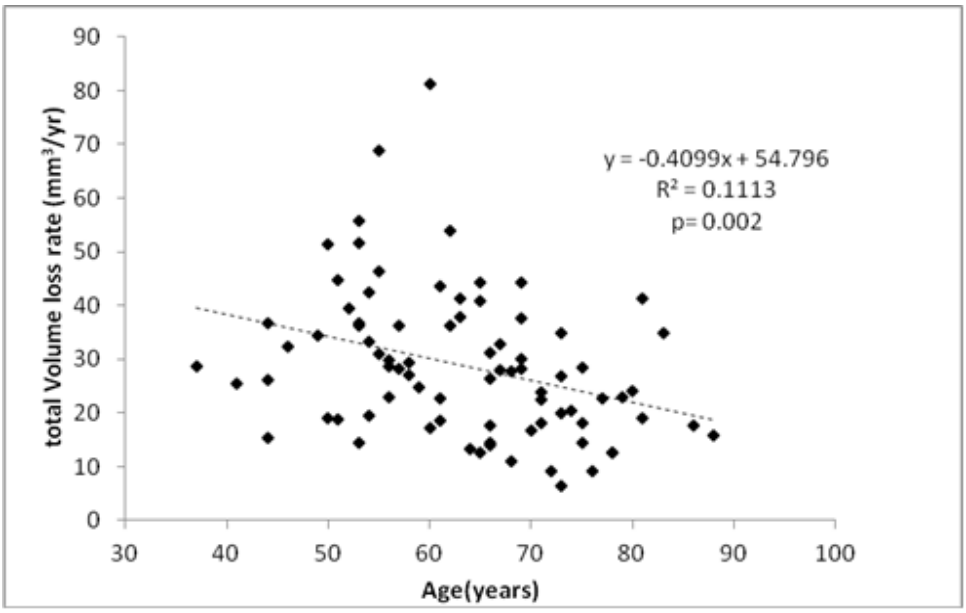

Figure 4.11 Correlation of total volume loss rate versus the age of the patient for 81 of the retrieved tibial inserts.

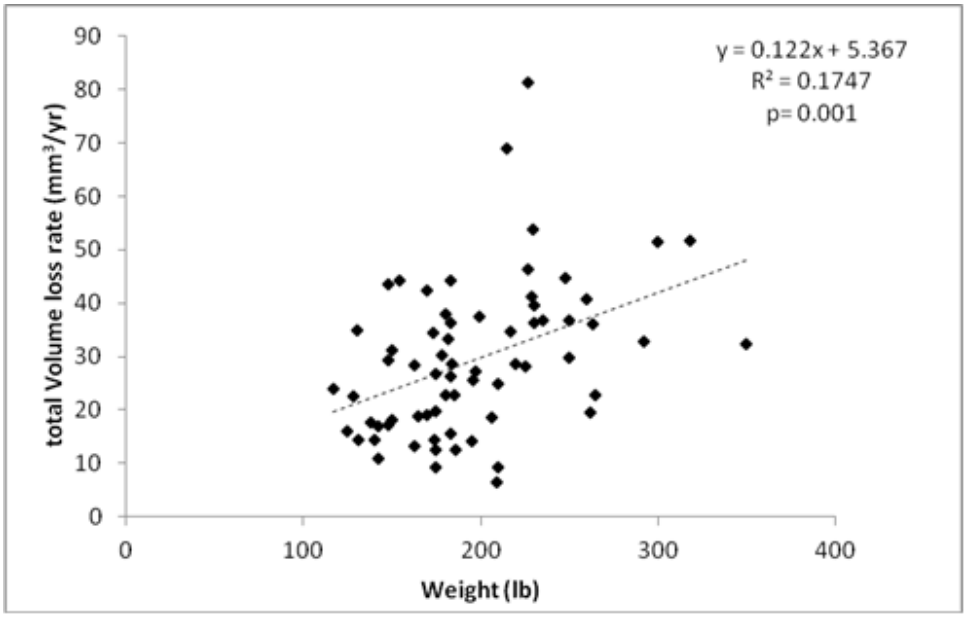

Figure 4.12 Correlation of total volume loss rate versus the weight for 67 of the retrieved tibial inserts.

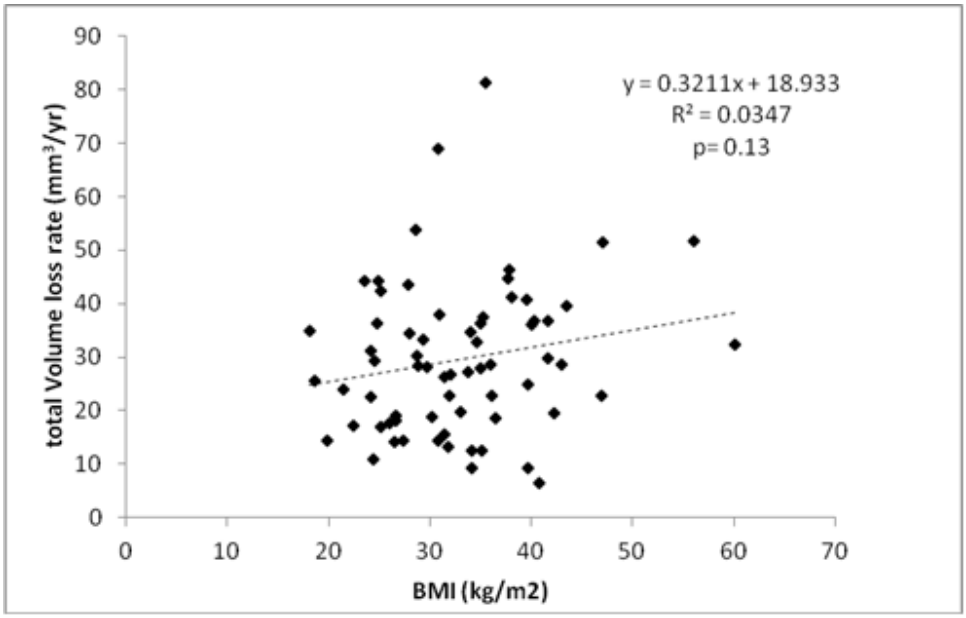

Figure 4.13 Correlation of total volume loss rate versus the BMI for 67 of the retrieved tibial inserts.

4.3 Aim 2: Determine the Structure and Impact of Striated Pattern on Wear

4.3.1 Is the Presence of Striated Pattern an Indicator for Wear Scar?

Striated patterns usually appear centrally on the wear scars and are mostly in antero-posteriorly directed, with elongated striations in the anterior region and shorter striation or random ones in the posterior part of the plateau.

In this aim, the striated patterns were observed on 61 out of 81 (frequency >75%) of the retrieved tibial insets. The striated patterns usually occurred on both the medial and lateral tibial plateaus. In this group of 61 retrieved tibial inserts, only one of a postmortem retrieved insert exhibited no striated pattern on the lateral side. As mentioned in chapter 3, all the outlines of the retrieved tibial inserts were normalized between [-1, 1], and all to the right side knee. The average percentage of the striated area in the total area of the tibial insert was determined for all 61 inserts (32.27% ± 17.33%, ranged: 1.00%-74.81%). For the medial and lateral tibial plateau,

the total medial or lateral articulating area was considered. Therefore, the percentage of the striated area was determined for each tibial plateau (15.45% ± 10.30%, range: 1.00%-49.55%, 16.81% ± 9.11%, and range: 0%-34.80%, respectively). There was a weak positive correlation between striated area and time *in situ*, wear volume loss and maximum linear penetration (R^2=0.07, p=0.02, R^2=0.07, p=0.03, R^2=0.006, p=0.03, respectively) (figure 4.14, 4.15 and 4.16).

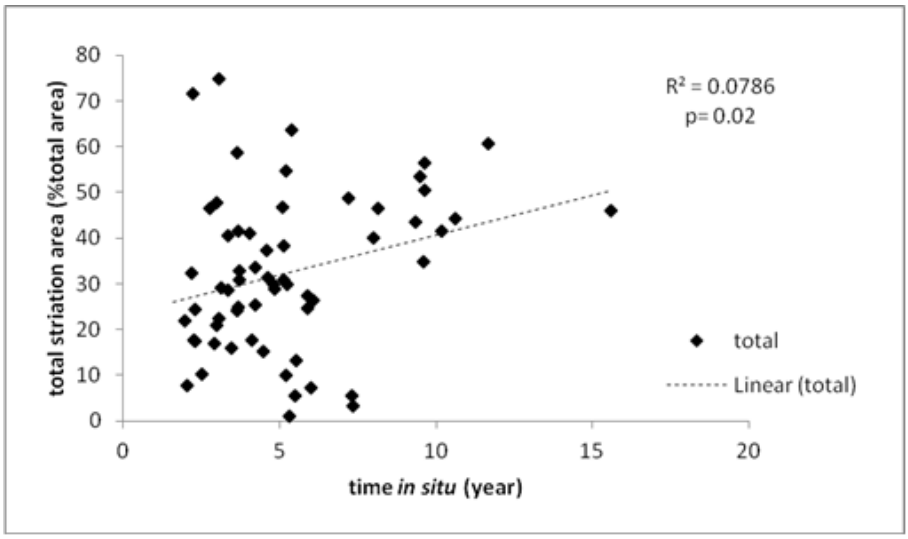

Figure 4.14 Correlation of the percentage of total striated area versus time in situ.

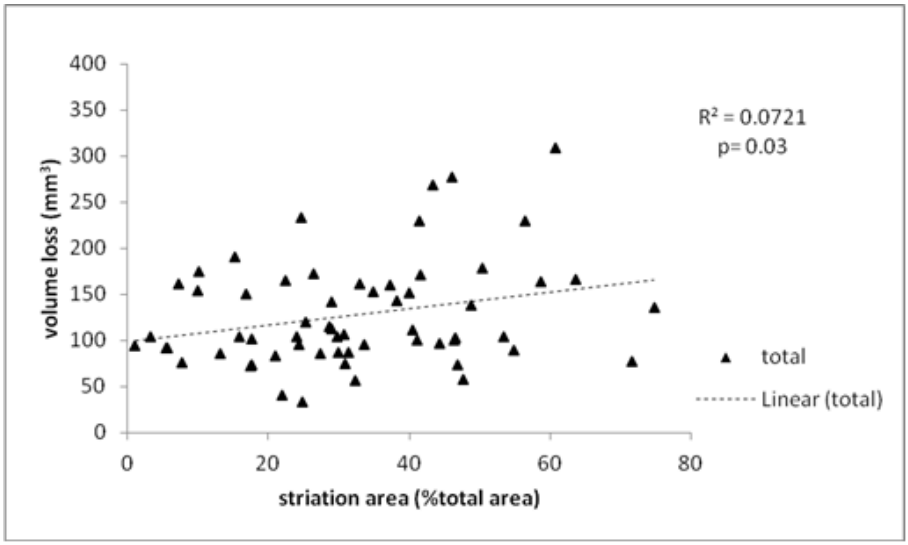

Figure 4.15 Correlation of the total volume loss versus the percentage of the total striated area of the tibial insert.

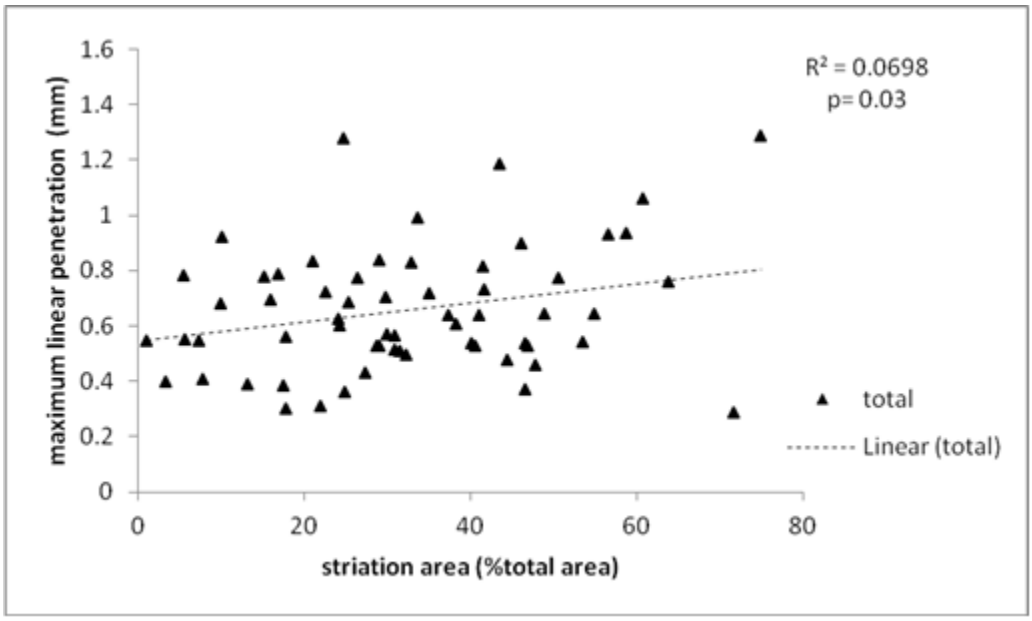

Figure 4.16 Correlation of the maximum linear penetration versus the percentage of the total striated area of the tibial insert.

Figure 4.17 shows the regression analysis of striated areas between medial and lateral plateau for 61 retrieved components. The ratio of the striated areas of lateral to medial is shown to be approximately 0.51 which indicates that the striated area on medial side is larger than on the lateral side. However, because of the positive intercept, this is only true once the striated area exceeds 20% of total plateau area. Statistically, there is a correlation of striated areas between both plateaus (R^2=0.33, $p<0.001$). According to paired t-test, there is no significant difference between medial and lateral striated areas ($p> 0.05$).

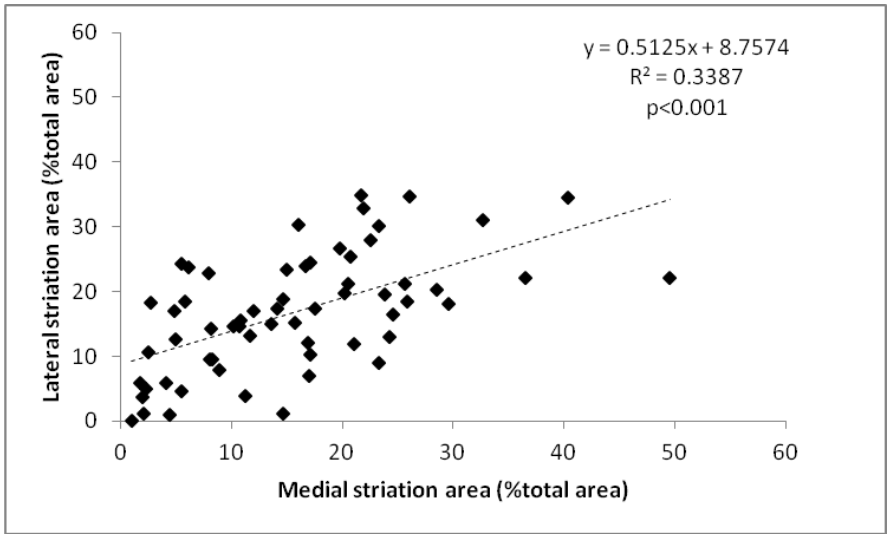

Figure 4.17 Regression analysis of lateral versus medial for striated areas.

The striated areas for all 61 tibial inserts were overlaid as shown in figure 4.18. Increasing the red scale intensity (darker) indicates more inserts had the striated pattern in a particular location. The striations, as displayed by the plot, are mostly located centrally and also near the side edge of the lateral plateau and in the medial side they mostly occur around the central region. In both medial and lateral plateau the striated patterns are spread more antero-posteriorly along the edges.

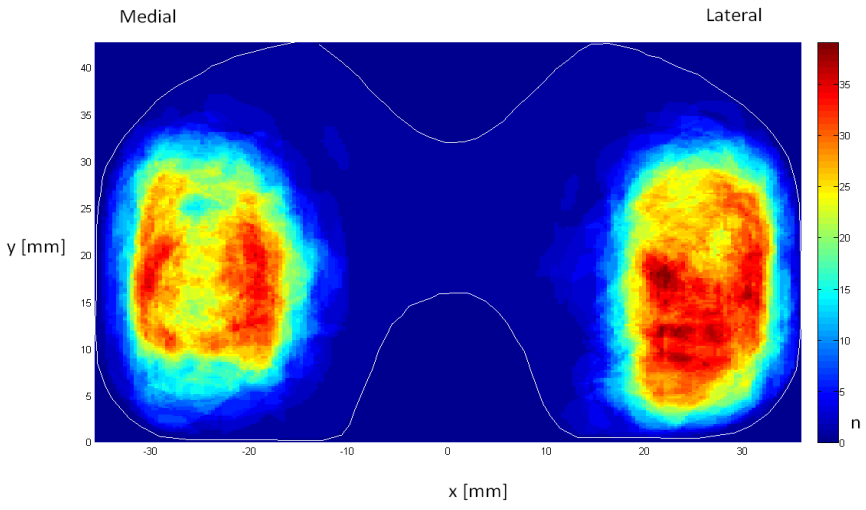

Figure 4.18 Overlay plot represents the striation areas for 61 retrieved inserts.

4.3.2 Crystallinity of Hill and Trough in Striated Patterns

4.3.2.1 Raman Spectroscopy Method

Raman Spectroscopy was used to determine the average value for the percentage of the orthorhombic content (crystallinity) for all four UHMWPEs test samples with various cooling methods (oven, air, liquid nitrogen, and water) with known crystallinity (figure 4.19). The calculated values for all four samples except for the one with water cooling method are slightly higher than the values given by Orthoplastic Ltd. A reasonable change of the crystallinity between the samples was noted. The difference in crystallinity between the two methods of DSC and Raman spectroscopy is significantly difference ($p<0.05$) except for the water cooling method sample.

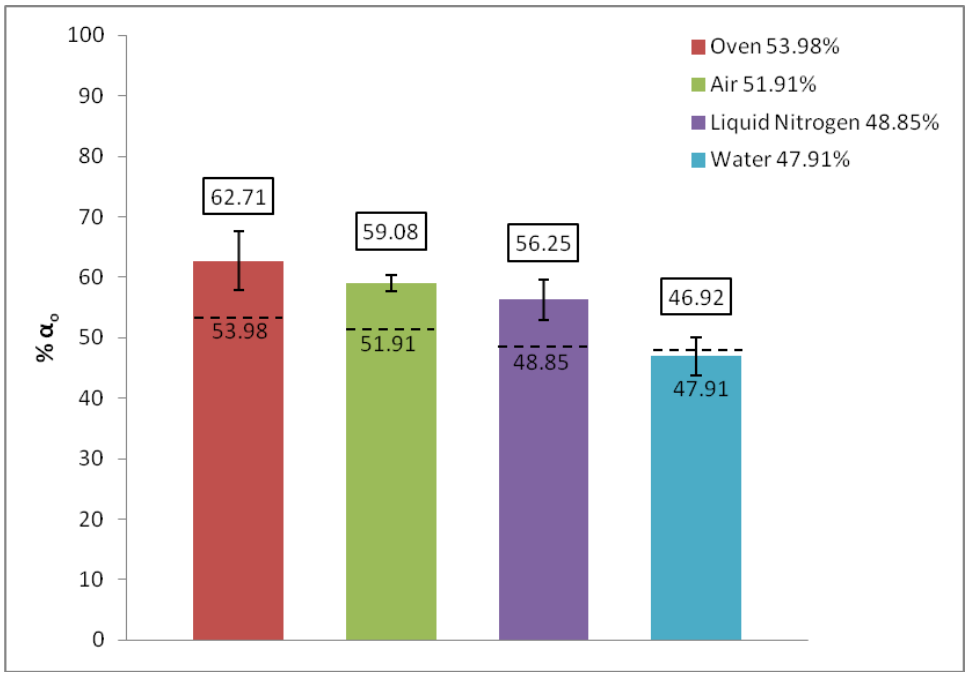

Figure 4.19 Degree of orthorhombic content in UHMWPE samples with known crystallinity, nominal values are shown with dashed lines, measured values are shown in the boxes.

To compare the difference in crystallinity between hills and troughs of the striated patterns, the average Raman spectra that were measured on the hills and troughs of the striated pattern on the retrieved UHMWPE insert are shown in figure 4.20. The assignment of the bands has been adapted from previous studies [59,78]. The bands at 1416 and 1130 cm^{-1} increased in intensity on the hill of the striated pattern compared to the trough, which confirms that these are the most sensitive bands to crystallinity changes [79]. The band at 1416 cm^{-1}, which relates to the bending of CH_2, is assigned for the crystalline phase and its intensity is proportional to the content of the orthorhombic phase (Eq1.1) [58,59,80]. The bands at 1440 and 1460 cm^{-1}, which are assigned to the amorphous phase, are slightly weaker in the hill of the striated pattern; therefore this trend indicates a higher crystallinity of the hill on the striation.

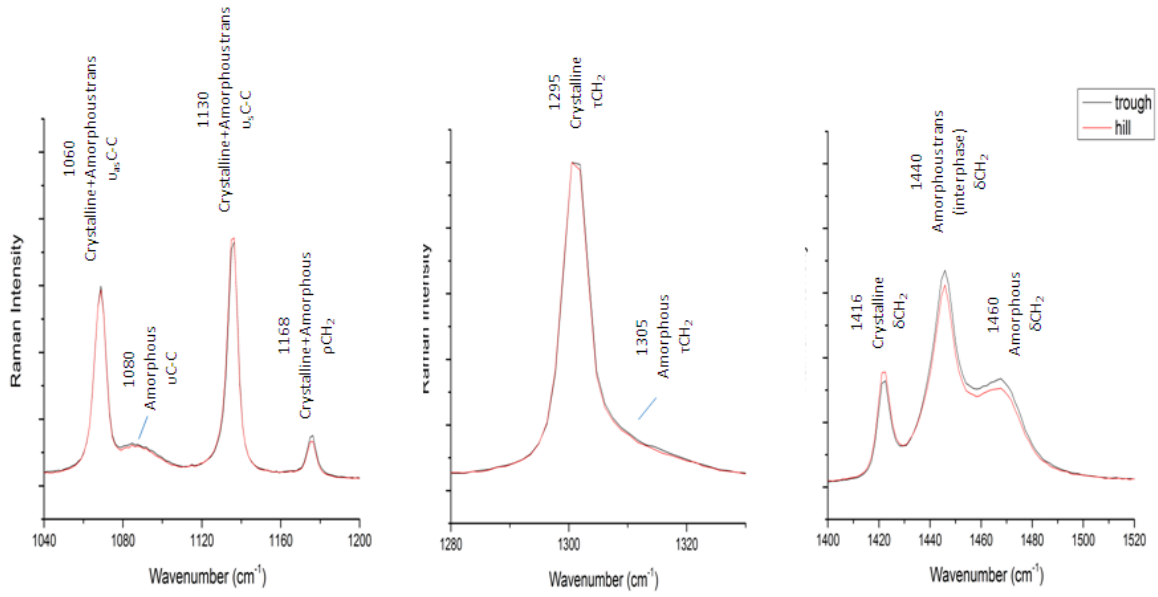

Figure 4.20 Average Raman spectra measured on the hill (red) and on the trough (black) of the striated pattern, the assignment of the bands is given in literature [52,59,81,82].

As mentioned in chapter 2, the fraction of orthorhombic (α_o), amorphous (α_a) and intermediate anisotropic disordered (α_b) phases were calculated according to Strobl and Hagedorn [59]. The mean values (± standard deviation) of α_o, α_a and α_b were calculated from the spectra. The data is shown in figure 4.21. The quantitative data are on agreement with the recorded qualitative data. The orthorhombic content on the hill is increase significantly ($p=0.001$) at the expense of the third phase content (α_b). The orthorhombic value (α_o) is 0.67±0.08 and 0.54±0.04 for the hill and trough, respectively. The amorphous content (α_a) is 0.18±0.04 for the hill, which is lower than for the trough (0.22±0.02). The third phase content (α_b) on the hill is significantly ($p= 0.01$) lower than the trough on the striation (0.13±0.09, 0.22±0.05, respectively), which shows that the intermediate phase content is decreased. This indicates a partial transformation from intermediate to the orthorhombic phase.

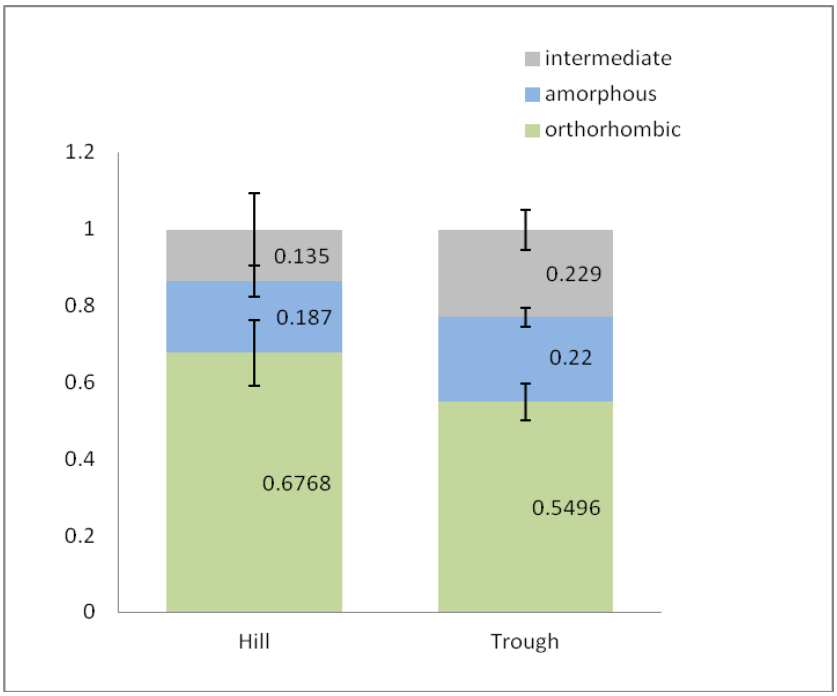

Figure 4.21 Mean values of α_o, α_a and α_b contents from the Raman spectra recorded on the hill and trough of the striated pattern.

The box plot for phase content on the hill and the troughs is shown in figure 4.22. The differences between hill and trough are statistically significant for each phase (α_o, p=0.001, α_a, p=0.03 and α_b, p=0.01).

The $I_{1416}/(I_{1440}+I_{1460})$ ratio is used to quantify the phase transformation from orthorhombic to monoclinic. Also, this ratio can represent the change of the setting angle of the orthorhombic lattice due to mechanical load (shear and/or compression). In the I_{1416}/I_{1295} ratio the intensity at 1295 cm^{-1} is independent of the conformation. Therefore, it can be used to determine the concentration changes of the orthorhombic phase. The changes of the 1416 cm^{-1} band may not only be due to the monoclinic phase presence, but also ill-defined orthorhombic crystalline structures such as dislocations, chain folding or disruption of the crystals [22,56].

To evaluate the occurrence of the orthorhombic to monoclinic phase transformation the intensity ratio of $I_{1416}/(I_{1440}+I_{1460})$ and I_{1416}/I_{1295} were calculated according to previous studies [48,56,78]. The intensities I_{1416}, I_{1440}, I_{1460} and I_{1295} were determined from the corresponding peak integrated areas.

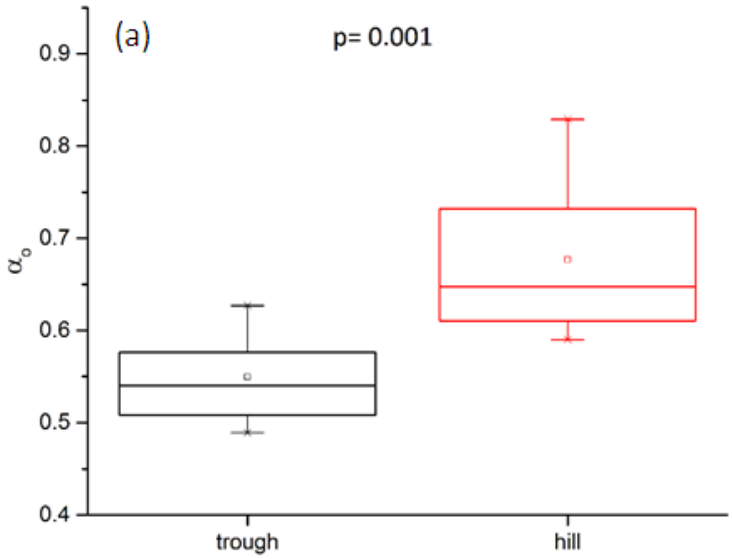

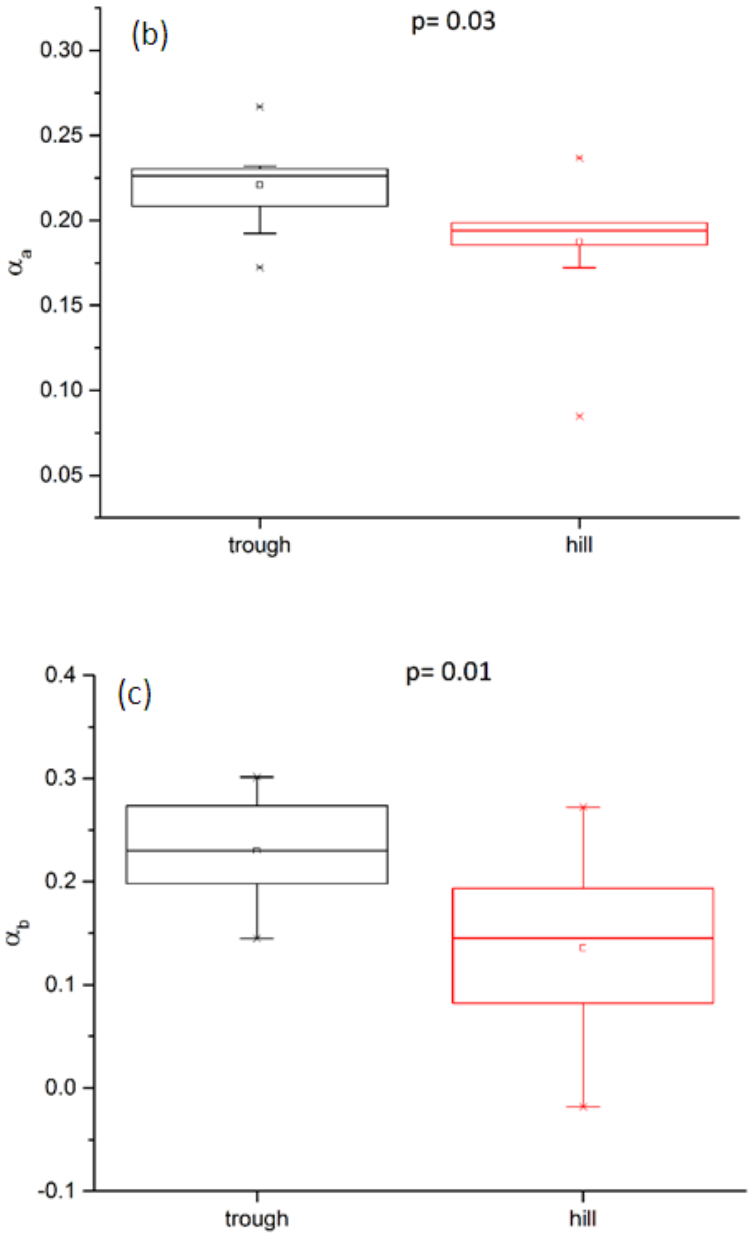

Figure 4.22 Box plot for a) α_o, b) α_a and c) α_b values for the hill and trough of the striated pattern.

The $I_{1416}/(I_{1440}+I_{1460})$ and I_{1416}/I_{1295} ratios were calculated for the hill and trough of the striated patterns (figure 4.23).

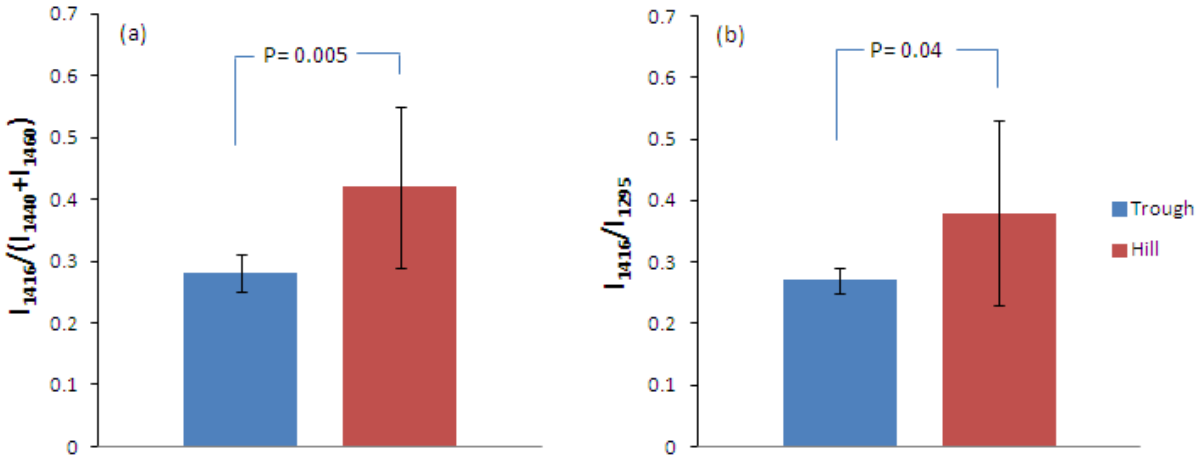

Figure 4.23 Mean values (± SD) of the a) $I_{1416}/(I_{1440}+I_{1460})$ and b) I_{1416}/I_{1295}. Intensity ratios calculated from the average Raman spectra on the hill and trough of the striated pattern.

Both ratios are significantly decreased in the trough of the striated pattern which shows that the concentration of orthorhombic crystallinity is lower in the trough compared to the hill. This is as expected according to the orthorhombic content (α_o), as it is decreased in the trough.

According to Edidin et al. [23], under loading conditions (uniaxial and multiaxial) the crystalline lamellae can be rearranged and result in an anisotropic lamellae orientation. To evaluate the residual strain on striated pattern on the UHMWPE insert, the full-width at half-maximum (FWHM) of the 1130 and 1060 cm^{-1} bands were calculated. To determine the molecular orientation, the ratio of I_{1130}/I_{1060} was calculated for both hill and trough of the striation. The bands at 1060 and 1130 cm^{-1} have different vibrational symmetries and I_{1130} becomes stronger if the molecules are oriented in a preferred direction with respect to I_{1060}

[51,56,83]. No significant differences were observed between hill and trough (1.32±0.15, 1.27±0.07, respectively) ($p>0.05$) (figure 4.24).

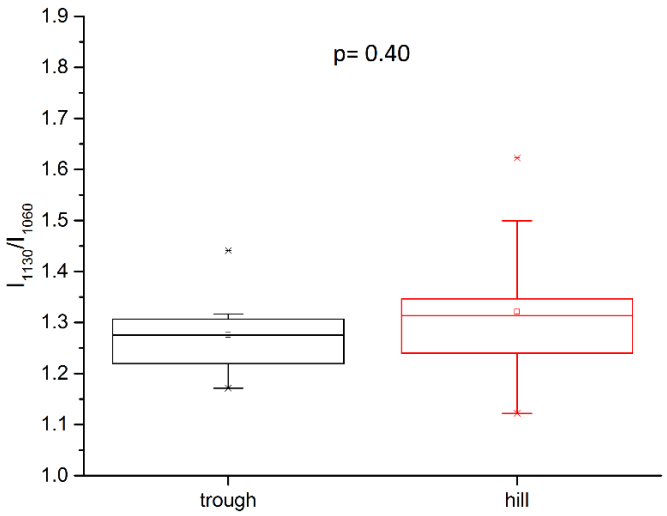

Figure 4.24 Box plot for the intensity ratio of I_{1130}/I_{1060} calculated from the Raman spectra on the hill and trough of the striated pattern.

The band at 1060 cm^{-1} (C-C antisymmetric stretching mode) and 1130 cm^{-1} (C-C symmetric stretching mode) can split into two components under compressive strain which causes the 1130 cm^{-1} band to become stronger compared to the 1060 cm^{-1} band [56]. The FWHM of the bands located at 1060 and 1130 cm^{-1} were measured in each Raman spectra. As shown in figure 4.25 there is no significant difference in FWHM between hill and trough within the striated pattern.

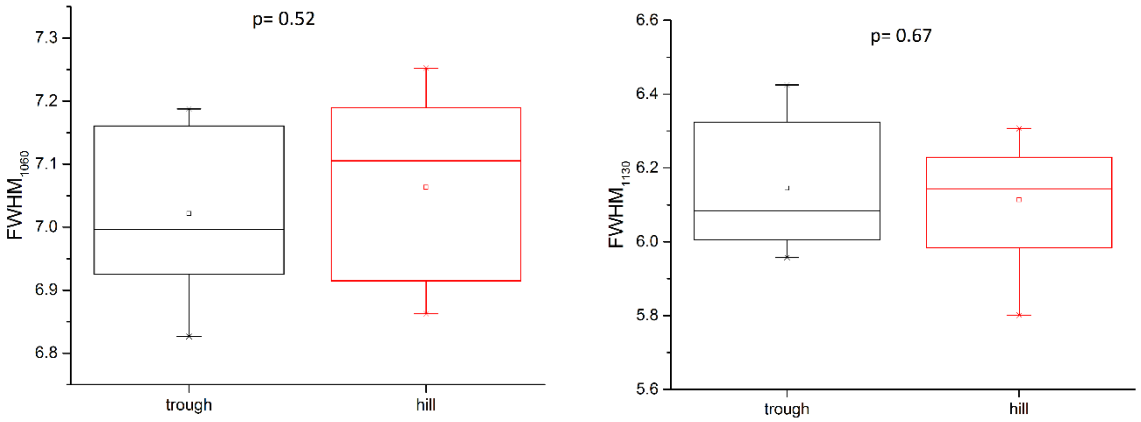

Figure 4.25 Box plot of the full-width at half-maximum (FWHM) of the bands at 1060 and 1130 cm^{-1}

By comparing the Raman spectra of the control sample with the retrieval, the shift of Raman bands to the higher wave number is observed. According to previous studies [84], this shift may occur due to compressive strain during *in situ* articulation of the knee joint. The difference shown in figure 4.26 is the representative spectra that compare a Raman spectrum of the known crystallinity sample (air) with a spectrum of the hill on the striation of the retrieved sample.

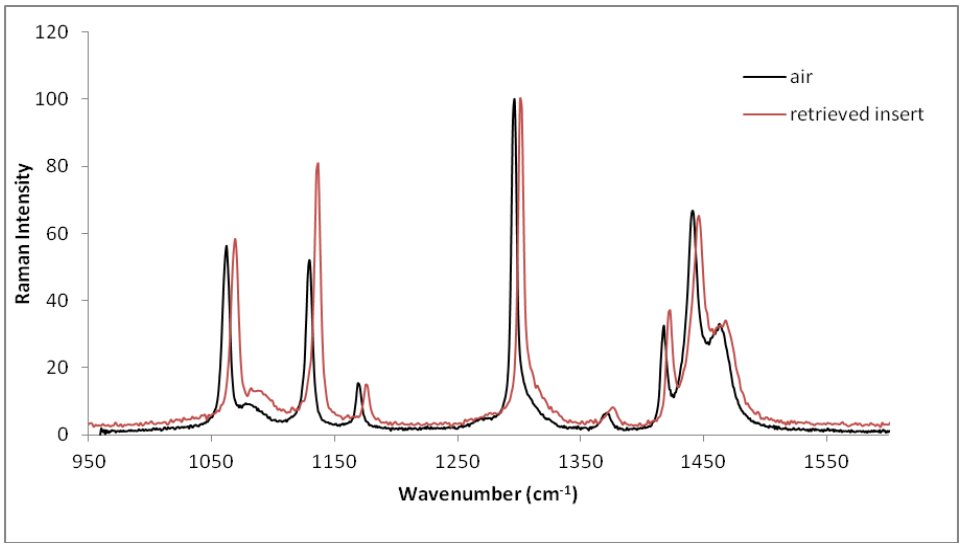

Figure 4.26 Comparison of a Raman spectrum of a sample with known crystallinity to that of a retrieved insert.

4.3.2.2 ATR-FTIR Method

In this study, the quantification of the polyethylene crystallinity with ATR-FTIR is performed according to Zerbi et al. [70] by determining the spectral features in the region of 680-780 cm^{-1}. Figure 4.27 shows a representative IR spectrum of one of the PE samples with known crystallinity (UHMWPE, water cooling method), by zooming into the 680-780 cm^{-1} region, the two peaks at 720 and 730 cm^{-1} can be distinguished more clearly (figure 4.29) as described earlier these two peaks are related to the crystalline phase.

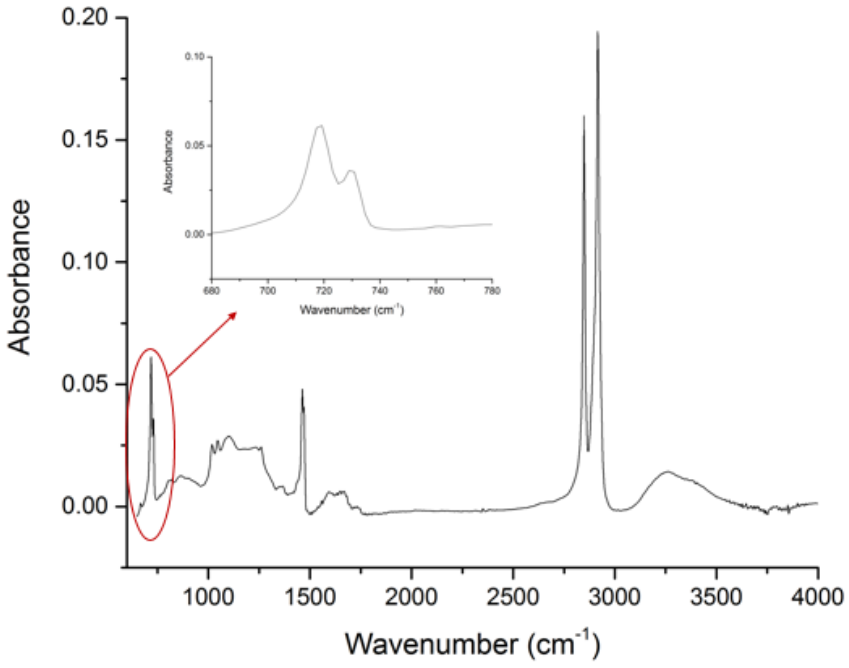

Figure 4.27 IR spectrum of UHMWPE control made by water cooling method.

The average crystallinity for all four control samples with different cooling methods (oven, air, liquid nitrogen and water) is plotted in figure 4.28. The calculated values for all four samples are lower than the given values by Orthoplastic Ltd. in spite of the reasonable trend which is decreasing especially for the last three samples (air, liquid nitrogen and water).

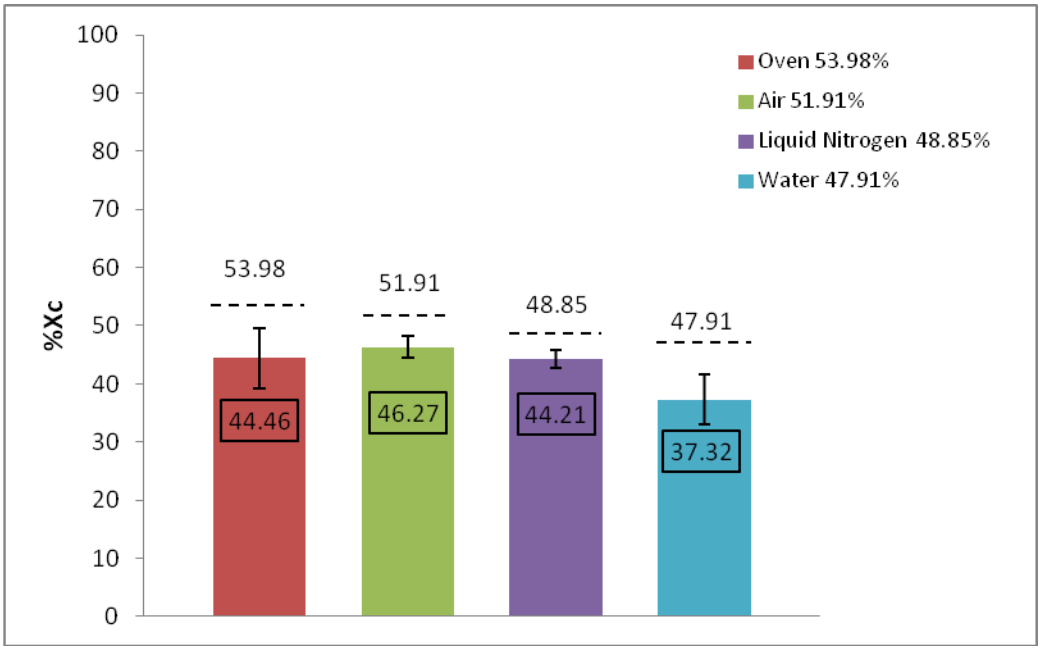

Figure 4.28 Degree of crystallinity in control samples, nominal values are shown with dashed lines, measured values are shown in the boxes.

The comparison of the Raman and the ATR-FTIR techniques for the evaluation of the crystallinity content on the four control samples (figure 4.19 and figure 4.28) shows that the Raman technique gives a higher value compared to the ATR-FTIR. The same trend of the crystallinity content can be observed with both techniques. The difference in crystallinity between the two methods is statistically significant ($p<0.05$, student t-test).

In order to analyze the crystallinity of the troughs and hills of the striated patterns, the same retrieved tibial insert that was analyzed with Raman spectroscopy with the dominant feature of striations in both the medial and the lateral plateau was examined by means of ATR-FTIR. To evaluate the crystallinity of the hill and trough, 9 and 3 measurements were done respectively. As shown in the figure 4.29, no significant differences were observed between the

hill and trough on the striated pattern although the results suggest that the hills have a slightly higher crystallinity compared to the troughs of the striated pattern.

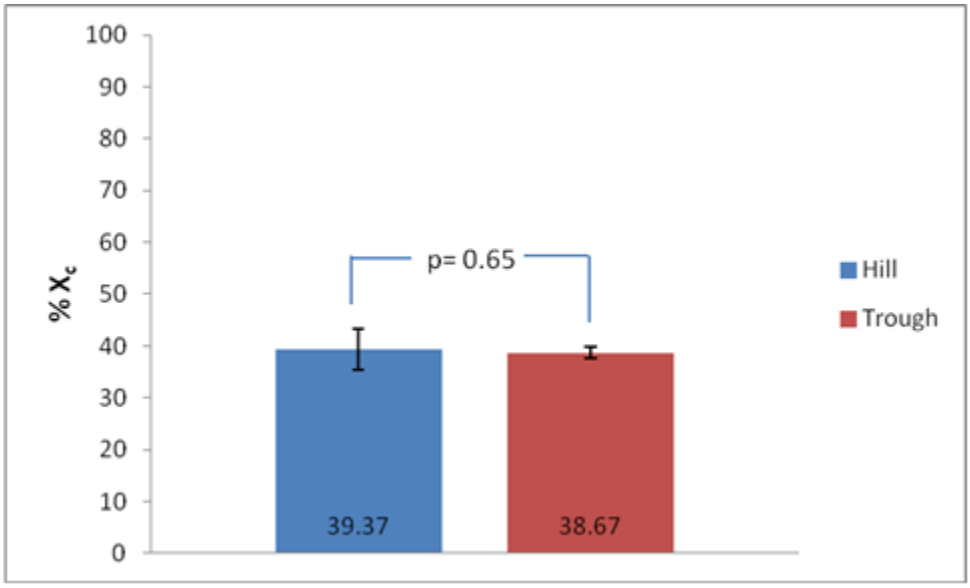

Figure 4.29 Degree of crystallinity on the hill and trough of the striated pattern in the retrieved insert.

Chapter 5. Discussion

The purpose of specific aim 1 in this study was to determine the accurate *in vivo* wear rate for one specific knee implant design (NexGen, CR). Therefore, the tibial insert of 81 patients were evaluated and measured with a CMM. The wear volume was determined with an autonomous mathematical reconstruction method [11]. The resulting wear rate was determined as 13.81±2.04 mm^3/year. This value is lower than most other retrieval studies [33,36,85–88]. However, most of these studies did not account for creep as confounding factor. *In vivo*, patient activities as well as other patient and surgeon specific factors contribute to the final outcome. The higher wear rates determined in other studies can be explained. First of all, some of these studies were performed on other implant systems and older polyethylene material that was prone to oxidation and higher wear. Second, there is no other study that uses a sophisticated method as established by Knowlton et al. [11]. Other values were determined by approximations based on linear wear measurements or radiographs [8,9,35,36,75]. Third, some studies considered backside wear as well, which leads to a higher wear rate [35,89,90]. Here, backside wear was not considered; therefore the volumetric wear rate is lower than reported in other studies [89]. The corrected values for the average volumetric wear rate in the medial and lateral tibial plateau are 6.09±5.93 and 7.07±8.94 mm^3/years, respectively. This is in agreement with one study that has shown the same wear for both medial and lateral compartments [91]. However, have shown that the medial compartment exhibits a higher wear rate compared to the lateral side [38,85,92,93]. The results show that volume loss is increasing with time *in situ* for medial, lateral and total articular surfaces, which is in a good agreement with other studies [91,93,94]. In Table VI, the *in vivo* and *in vitro* wear assessments of some other studies are shown.

Table VII. COMPARISON OF KNEE WEAR ASSESSMENT BOTH *IN VIVO* AND *IN VITRO* OF OTHER STUDIES

	Study	**Implant design**	**Assessment method *in vitro***	**Volume loss rate [mm^3/year]. [mm^3/Mc]**	**Linear penetration rate [mm/year]**
in vivo	Kop et al. [85]	MB-APG	CMM	85	
	Atwood et al. [36]	MB-LCS	Through-thickness	54	
	Engh et al. [87]	FB-CR/PS	Through-thickness	74±49	
	Benjamin et al. [86]	FB-CR-AMK	laser scan	794	0.35
	Berry et al. [35]	FB-Sigma	Through-thickness		0.07
	Crowninshield et al. [95]	FB-NexGen	visual rating of damage mode		0.0041
	Lavernia et al. [88]	FB-CR-PCA	Through-thickness	32±43	0.12±0.10
	Gill et al. [96]	FB-CR-AGC	RSA	100	0.1
	Teeter et al. [89]	FB-PS-Genesis II	Micro-CT		0.05
	Knowlton et al. [16]	FB-CR-MGII	CMM-Autonomous mathematical reconstruction	13.0±2.9	
	Current study	FB-CR-NexGen	CMM-Autonomous mathematical reconstruction	13.81±2.04	0.03
in vitro	Muratoglu et al. [97]	FB-CR		23± 6	
	Schwenke et al. [98]	FB-CR-MGII	Gravimetric analysis	22.4 (load control)-9.8 (displacement control)	
	Teeter et al. [90]	FB-CR-Genesis II	Micro-CT	24.7	
	Laurent et al. [99]	FB-CR-NexGen	Gravimetric analysis	15.4±1.2	
	Popoola et al. [100]	FB-CR-NexGen	Gravimetric analysis	15.4±3 (displacement control)	

MB= Mobile Bearing, FB= Fixed bearing, CR= Cruciate retaining, PS= Posterior stabilized

The maximum linear penetration rate after creep correction for the medial and lateral tibial plateau is 0.015 and 0.017 mm/year, respectively. Interestingly, this result is in good agreement with Lavernia et al. [88] who have shown the similar linear penetration in medial and lateral compartment. However, the result is in disagreement with a study that shows the linear penetration is higher on the medial side compared to the lateral side [101]. The good linear relationship between total volume loss rate and maximum linear penetration rate (R^2=0.61,

p<0.001) suggests that maximum linear penetration might a good surrogate for wear volume. However, by plotting the volume loss versus maximum linear penetration of each tibial plateau and considering the 95% prediction bands for each individual component (figure 5.1 (a) and (b)), it can be concluded that there is very high uncertainty in obtaining the wear volume from individual measurements, despite the good global correlation. For instance, the penetration of 0.6 mm on the medial side correlates to the wear volume of 60 to 160 with regard to the 95% prediction confidence interval. The large uncertainty might be because the location of the thickness minima after wear does no longer coincide with the manufactured minimum of this device. In conclusion, the results suggest that penetration is only a good surrogate measure for large cohort studies.

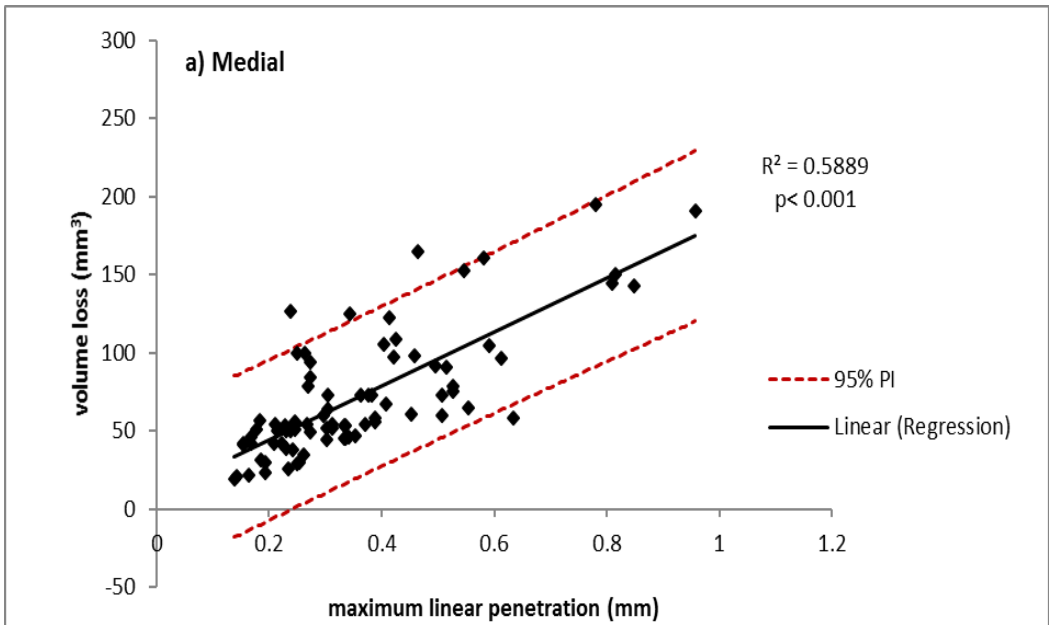

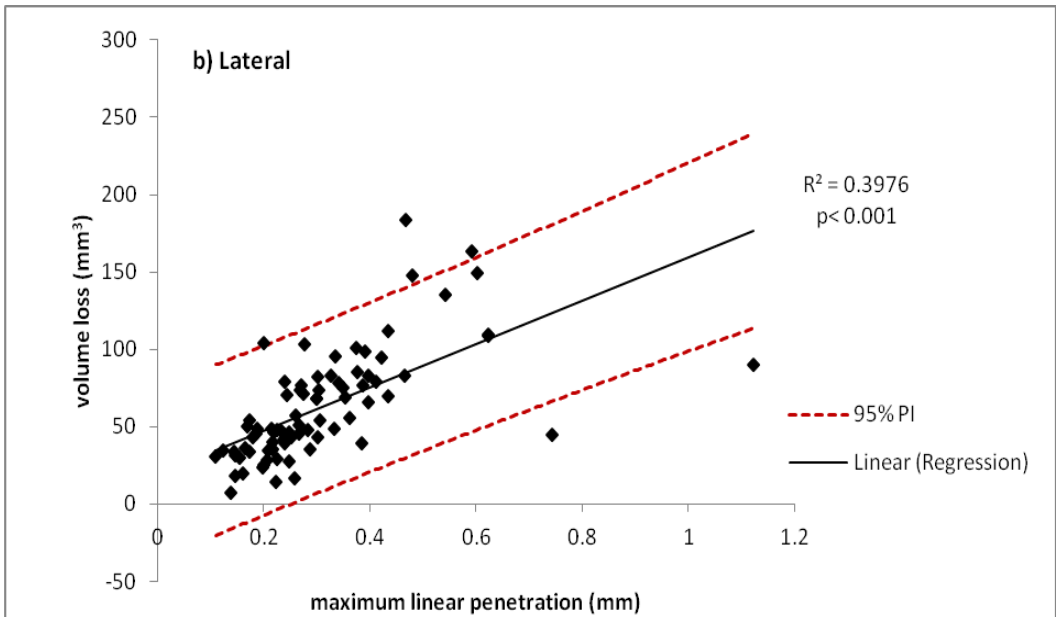

Figure 5.1 Correlation of a) medial and b) lateral volume loss versus maximum linear penetration for retrieved tibial inserts.

Although, the wear scar area has been used as a wear rate surrogate in several studies [37,38,85]; our results show no correlation is observed between the volume loss rate and the percentage of the wear scar area (R^2=0.008, p=0.49).

According to figure 4.15, which shows the boxplot for the four sizes of available implants, there is no significant difference between wear rate and implant size in this study. Thus, in this study, implant size did not have an impact on volume loss rate, contrary to observations by Affatato et al. [47] who compared the *in vitro* wear rate of two different sizes (small and large) of mobile inserts and found that the larger implant generated twice the wear volume of the smaller size implant applying equal loads.

The second research question in aim 1 was: 'Which patient factors impact wear'. It was shown for the entire subject group that age and gender were significant impact factors. Age has been suggested to be a surrogate measure for patient activity. Thus, a decrease in wear rate with

increasing patient age is not surprising. Also, female patients are associated with lower wear of tibial inserts. There can be several reasons for that including: a lower average weight, lower activity level or potential anatomical factors. The exact reasons would have to be further investigated. Interestingly, by including patient weight both other factors lost their significance. This means that the load applied to joint by additional weight is the most important impact factor on volumetric wear between the three factors. The reasons that gender lost significance may be that weight and patient age are confounding factors to a certain degree. However, there are several other factors which could impact the polyethylene wear rate which are not considered here, such as implant alignment (posterior tibial slope, etc.) and knee scores. It is possible that such factors will account for some of the variance leading to a better model. Also, by increasing the patient group factors like age and gender may gain significance again.

The first research question of aim 2 was if the presence of a striated pattern is an indicator for wear. In order to answer this question the percentage of the tibial insert surface exhibiting the striated pattern was quantified by means of a CMM. To investigate if the presence of the striated pattern is an indicator for wear scar, the calculated volume loss and maximum linear penetration were correlated with the percentage of area exhibiting striations. The size of striated area and wear volume were correlated, although not strongly. Knowlton et al. [16] showed that the striated pattern was the best wear predictor of all occurring wear patterns. Thus, a higher correlation could have been expected.

The second research question was if striations have a higher crystallinity due to re-organization of PE molecules during wear. Therefore, Raman spectroscopy and ATR-FTIR analyses were carried out to investigate the structure of the striated patterns in one of the retrieved tibial inserts with dominant striation features. Although the occurrence of the striated

pattern on retrieved tibial inserts in other studies has been reported [15,16]; to our knowledge, no study describes in detail the structure of these patterns. However, there is considerable literature on the morphology and crystallinity changes of the articulating surfaces of the UHMWPE components. Both methods, FTIR and Raman, have been widely used to investigate the morphology of the UHMWPE both *in vivo* and *in vitro* and various studies [51,59,83] have tried to correlate the intensities of the marker bands for the PE samples with their crystallinity.

In this study, the hypothesis was that the hills on striated patterns are more crystalline compared to the troughs since the loads on the articulating surface could cause rearrangment of UHMWPE lamellae on the surface. For the known crystalline samples, which are used as a contol for the method, although the Raman spectroscopy results are slightly higher than the reported ones, it shows the right trend of the crystallinity amount for the samples. The higher crystallinity values in Raman spectroscopy compared to the reported DSC values is consistent with Dothee et al. [80], but in contrast to Kyomoto et al. [50], who shows Raman crystallinity measurements are lower than that of DSC. The latter study reports the possibility of the presence of other crystalline phases. In addition, the difference of the measured values may be due to assessment of the baseline and curve fitting method. Although the total evaluated values would be affected but the trend would stay the same.

According to Raman spectroscopy results on the striated patterns on the retrieved tibial insert, the average crystalline content (α_o) of the hills is significantly ($p=0.001$) greater than that of the troughs, which may due to the mechanical stress. This is in accordance with the Eddidin et al. [23] study which showed the crystalline lamellae of the UHMWPE oriented near the articulating surface during the *in vitro* wear test due to the applied load. Also, a study by Affatato et al. [47] compared the morphology and load patterns of two sizes of UHMWPE inserts by

means of micro-Raman spectroscopy. They have obsereved that the smaller contact area on the surface of implants with a smaller size exhibit more crystallinity changes compared to larger sized areas under the same amount of load. In our study, the calculated amorphous content (α_a) for the hill is significantly ($p= 0.03$) lower than that of the trough. This result can be explained by the Galetz et al. [40] study, which elucidates that the frictional load reduces the intensity of the crystalline assigned band (1416 cm^{-1}) and adhesive interaction in the articulating surface can change the order in the crystalline phase and increase the amorphous content. In addition, the significant decrease of the two ratios of $I_{1416}/(I_{1440}+I_{1460})$ and I_{1416}/I_{1295} on the trough of the striated pattern show that the concentration of orthorhombic crystallinity is lower in the trough compared to the hill, which matches with the finding of increased orthorhombic content (α_o) in the hill.

Crystallinity evaluation under the FTIR method is still controversial. According to literature [65,69,70,73,102], there is no consistent method for the quantification of crystallinity available. In this study, we used the method by Zerbi et al. [13]. In the Minn et al. [102] study, they have described the method to quantify the crystallinity by considering the area under the peaks of 719 and 729 cm^{-1} bands and dividing by the overall area in this region. This method does not seem as accurate since they have considered the amorphous band roughly in the negative peak between 719 and 729 cm^{-1} bands. In the Costa et al. [73] study, they reported the crystalline band at 1896 cm^{-1} and an amorphous one at 1305 cm^{-1} and they have determined the crystallinity as a relation between these two peaks. The intensity of mentioned peaks were too weak in the ATR-FTIR spectrum to be evaluated in curve fitting in our study. In the Hagemman et al. [69] study, they reported that the band at 723 cm^{-1} is associated to the amorphous band, which is hidden between two crystalline bands (722 and 730 cm^{-1}). Since finding the hidden

amorphous band is not easily achievable through the band fitting, we could not use this method in our study.

The crystallinity values that were obtained by ATR-FTIR are lower than the Raman spectroscopy values. This may be explained by the difference in magnification of Raman and ATR-FTIR (50X, 20X for Raman spectroscopy and ATR-FTIR, respectively) and evaluation of the crystallinity. Similarly, Raman spectroscopy differences may be related to the assessment of the baseline for the integration area and the proper beginning and ending point of the integration. Another reason for these differences can be the constant in the equations (2.1) and (2.7) that are used for Raman spectroscopy and the FTIR methods, respectively in this study. The constants for Raman and FTIR methods have been verified experimentally for 100% crystalline HDPE and commercial PE sample, respectively.

For the striated patterns in the UHMWPE retrieved tibial inserts there was no significant difference between the crystallinity of the hills and troughs by ATR-FTIR method. The difference of the magnification between Raman spectroscopy and ATR-FTIR methods can play a critical role in the quantification of the crystallinity. As mentioned in chapter 2, the width of a single striation is about 70 μm which is difficult to catch with a magnification of 20X with ATR-FTIR. In ATR-FTIR there is a direct contact between the sample and tip of the ATR crystal, therefore; for the Ge crystal with nominal diameter of 100 μm it is difficult to catch the striations with the width of 70 μm. In figure 5.2, the ATR-FTIR optical image on a stirated pattern has been shown. The Ge crystal mark illustrates that catching the hill on the striations is difficult; as shown the right side of the mark is on the trough area. Therefore, for these cases, Raman spectroscopy method has a greater advantage.

Figure 5.2 ATR-FTIR optical image and mark of the Ge crystal recorded on a striated pattern (hill and trough) on the articulating surface of the retrieved tibial insert.

In this study, although the ATR-FTIR has not shown any difference between the hill and trough in the striation structure, according to Raman spectroscopy results, the hill on the striations show higher crystallinity values compared to the trough, which is fulfill our hypothesis of specific aim 2.

Chapter 6. Limitation

This study has several limitations which should be considered. In both aims, only a specific tibial insert design and manufacturer has been evaluated, therefore; generalizability of the results needs to be demonstrated in future investigations. In the first aim, only a small population of patients was available. Also, not all clinical data were available for all patients. To investigate the impact of patient factors on wear, some other clinical data such as posterior tibial slope, Insall-Salvati, Blackburne-Peel ratio, etc. also need to be considered. In the applied method for the wear assessment, linear penetration and volume loss to wear and creep are indistinguishable.

In the second aim, only a small population of inserts with striated patterns was available. For the crystallinity measurements of the control samples only a small range of different crystallinity values (47.91%-53.98%) was available for this investigation. A higher range of UHMWPE crystallinity may provide a better evaluation of both the spectroscopy technique and also the assessment of the baseline and curve fitting. In this study, only one representative retrieved tibial insert was used to analyze the microstructure of the striated patterns, therefore; more retrieval inserts need to be investigated. To avoid the influence of oxidation and other environmental factors on the crystallinity measurement of the striations various retrieved tibial inserts with the same shelf age and time *in situ* are needed.

Chapter 7. Conclusion

Quantitative *in vivo* wear measurements of polyethylene tibial inserts will provide input for evaluation design and materials improvements of TKRs. Here, autonomous mathematical reconstruction algorithm [11] was applied to measure the wear volume change and maximum linear penetration of one specific tibial insert design (NexGen, CR). The results of this study suggest that maximum linear penetration and wear volume are well correlated, however are not an accurate surrogate for estimating wear volume of individual (single) TKR polyethylene components. A large cohort is necessary to obtain trust worthy wear rates from penetration measurements.

Patient factors can affect the performance of TKR. To analyze the impact of patient demographics on wear rate, factors cannot be considered in isolation. In this study, by considering age, gender and weight/BMI, patient weight had the most impact on the wear rate.

Also, quantifying wear area can be helpful to understand the influence of wear patterns on the wear rate. In this study striated patterns were analyzed and according to the results, the size (area) of the striated features is only weakly related to the amount of wear.

Raman spectroscopy and ATR-FTIR techniques were used to understand the structural changes at molecular level of the striated pattern and its impact on the wear behavior. The data reported in this study show that Raman spectroscopy was a more effective tool to analyze the microstructure of the striated pattern. The obtained results suggest that the crystallinity of the striated pattern in that the hills have a higher degree of crystallinity than troughs.

Chapter 8. References

[1] Kurtz SM, Lau E, Ong K, Zhao K, Kelly M, Bozic KJ. Future Young Patient Demand for Primary and Revision Joint Replacement: National Projections from 2010 to 2030. Clin Orthop 2009;467:2606–12. doi:10.1007/s11999-009-0834-6.

[2] Kurtz SM. Chapter 8 - The Clinical Performance of UHMWPE in Knee Replacements. In: Kurtz SM, editor. UHMWPE Biomater. Handb. Second Ed., Boston: Academic Press; 2009, p. 97–116.

[3] Gallo J, Goodman SB, Konttinen YT, Wimmer MA, Holinka M. Osteolysis around total knee arthroplasty: a review of pathogenetic mechanisms. Acta Biomater 2013;9:8046–58. doi:10.1016/j.actbio.2013.05.005.

[4] Thiele K, Perka C, Matziolis G, Mayr HO, Sostheim M, Hube R. Current Failure Mechanisms After Knee Arthroplasty Have Changed: Polyethylene Wear Is Less Common in Revision Surgery. J Bone Jt Surg 2015;97:715–20. doi:10.2106/JBJS.M.01534.

[5] Sharkey PF, Hozack WJ, Rothman RH, Shastri S, Jacoby SM. Insall Award paper. Why are total knee arthroplasties failing today? Clin Orthop 2002:7–13.

[6] Lonner JH, Siliski JM, Scott RD. Prodromes of failure in total knee arthroplasty. J Arthroplasty 1999;14:488–92.

[7] Blunn GW, Joshi AB, Minns RJ, Lidgren L, Lilley P, Ryd L, et al. Wear in retrieved condylar knee arthroplasties: A comparison of wear in different designs of 280 retrieved condylar knee prostheses. J Arthroplasty 1997;12:281–90. doi:10.1016/S0883-5403(97)90024-3.

[8] Collier MB, Engh CA, Hatten KM, Ginn SD, Sheils TM, Engh GA. Radiographic assessment of the thickness lost from polyethylene tibial inserts that had been sterilized differently. J Bone Joint Surg Am 2008;90:1543–52. doi:10.2106/JBJS.G.00651.

[9] Goldvasser D, Marchie A, Bragdon LK, Bragdon CR, Weidenhielm L, Malchau H. Incidence of Osteolysis in Total Knee Arthroplasty. J Arthroplasty 2013;28:201–6. doi:10.1016/j.arth.2012.06.008.

[10] Muratoglu OK, Perinchief RS, Bragdon CR, O'Connor DO, Konrad R, Harris WH. Metrology to quantify wear and creep of polyethylene tibial knee inserts. Clin Orthop 2003:155–64. doi:10.1097/01.blo.0000063604.67412.04.

[11] Knowlton CB, Wimmer MA. Autonomous Mathematical Reconstruction of Polyethylene Tibial Inserts to Measure Low Wear Volumes. J Biomed Mater Res B Appl Biomater 2013;101:449–57. doi:10.1002/jbm.b.32782.

[12] Gill GS, Joshi AB. Long-term results of Kinematic Condylar knee replacement AN ANALYSIS OF 404 KNEES. J Bone Joint Surg Br 2001;83-B:355–8. doi:10.1302/0301-620X.83B3.11288.

[13] Rand JA, Trousdale RT, Ilstrup DM, Harmsen WS. Factors Affecting the Durability of Primary Total Knee Prostheses. J Bone Jt Surg 2003;85:259–65.

[14] Hood RW, Wright TM, Burstein AH. Retrieval analysis of total knee prostheses: A method and its application to 48 total condylar prostheses. J Biomed Mater Res 1983;17:829–42. doi:10.1002/jbm.820170510.

[15] Wimmer MA, Andriacchi TP, Natarajan RN, Loos J, Karlhuber M, Petermann J, et al. A striated pattern of wear in ultrahigh-molecular-weight polyethylene components of Miller-Galante total knee arthroplasty. J Arthroplasty 1998;13:8–16.

[16] Knowlton C. Relationship of Polyethylene Surface Damage and Volumetric Wear in Retrieved TKA Liners, 2014.
[17] Kurtz SM. Chapter 7 - The Origins and Adaptations of UHMWPE for Knee Replacements. In: Kurtz SM, editor. UHMWPE Biomater. Handb. Second Ed., Boston: Academic Press; 2009, p. 81–95.
[18] Mow VC, Hayes WC. Basic orthopaedic biomechanics. Raven Press; 1991.
[19] Ayers DC. Maximizing ultra high molecular weight polyethylene performance in total knee replacement. Instr Course Lect 2001;50:421–9.
[20] Batchelor AW. Service characteristics of biomedical materials and implants. London : Singapore ; River Edge, NJ: Imperial College Press ; Distributed by World Scientific Pub; 2004.
[21] Wimmer MA. Wear of the Polyethylene Component Created by Rolling Motion of the Artificial Knee Joint. Ph.D. Dissertation. Technical University of Hamburg-Harburg, 1999.
[22] Tozzi S, Modena E, Falcioni S, Sudanese A, Affatato S, Taddei P. The effects of contact area and applied load on the morphology of in vitro worn ultra-high molecular weight knee prostheses: a micro-Raman and gravimetric study. J Raman Spectrosc 2014;45:781–7. doi:10.1002/jrs.4545.
[23] Edidin AA, Pruitt L, Jewett CW, Crane DJ, Roberts D, Kurtz SM. Plasticity-induced damage layer is a precursor to wear in radiation-cross-linked UHMWPE acetabular components for total hip replacement. Ultra-high-molecular-weight polyethylene. J Arthroplasty 1999;14:616–27.
[24] Kurtz SM. Chapter 1 - A Primer on UHMWPE. In: Kurtz SM, editor. UHMWPE Biomater. Handb. Second Ed., Boston: Academic Press; 2009, p. 1–6.
[25] Muratoglu OK. Chapter 13 - Highly Crosslinked and Melted UHMWPE. In: Kurtz SM, editor. UHMWPE Biomater. Handb. Second Ed., Boston: Academic Press; 2009, p. 197–204.
[26] Kurtz SM. Chapter 2 - From Ethylene Gas to UHMWPE Component: The Process of Producing Orthopedic Implants. In: Kurtz SM, editor. UHMWPE Biomater. Handb. Second Ed., Boston: Academic Press; 2009, p. 7–19.
[27] Kurtz SM. Chapter 3 - Packaging and Sterilization of UHMWPE. In: Kurtz SM, editor. UHMWPE Biomater. Handb. Second Ed., Boston: Academic Press; 2009, p. 21–30.
[28] Roe RJ, Grood ES, Shastri R, Gosselin CA, Noyes FR. Effect of radiation sterilization and aging on ultrahigh molecular weight polyethylene. J Biomed Mater Res 1981;15:209–30. doi:10.1002/jbm.820150209.
[29] Schmalzried TP, Callaghan JJ. Wear in total hip and knee replacements. J Bone Joint Surg Am 1999;81:115–36.
[30] Purdue PE, Koulouvaris P, Nestor BJ, Sculco TP. The Central Role of Wear Debris in Periprosthetic Osteolysis. HSS J 2006;2:102–13. doi:10.1007/s11420-006-9003-6.
[31] Callaghan JJ, Rosenberg AG, Rubash HE. The Adult Hip. Lippincott Williams & Wilkins; 2007.
[32] Harman MK, Banks SA, Hodge WA. Polyethylene damage and knee kinematics after total knee arthroplasty. Clin Orthop 2001:383–93.
[33] Gill HS, Waite JC, Short A, Kellett CF, Price AJ, Murray DW. In vivo measurement of volumetric wear of a total knee replacement. The Knee 2006;13:312–7. doi:10.1016/j.knee.2006.04.001.

[34] McGloughlin TM, Kavanagh AG. Wear of ultra-high molecular weight polyethylene (UHMWPE) in total knee prostheses: a review of key influences. Proc Inst Mech Eng [H] 2000;214:349–59.
[35] Berry DJ, Currier JH, Mayor MB, Collier JP. Knee wear measured in retrievals: a polished tray reduces insert wear. Clin Orthop 2012;470:1860–8. doi:10.1007/s11999-012-2248-0.
[36] Atwood SA, Currier JH, Mayor MB, Collier JP, Van Citters DW, Kennedy FE. Clinical Wear Measurement on Low Contact Stress Rotating Platform Knee Bearings. J Arthroplasty 2008;23:431–40. doi:10.1016/j.arth.2007.06.005.
[37] Grochowsky JC, Alaways LW, Siskey R, Most E, Kurtz SM. Digital photogrammetry for quantitative wear analysis of retrieved TKA components. J Biomed Mater Res B Appl Biomater 2006;79:263–7. doi:10.1002/jbm.b.30537.
[38] Harman MK, DesJardins J, Benson L, Banks SA, LaBerge M, Hodge WA. Comparison of polyethylene tibial insert damage from in vivo function and in vitro wear simulation. J Orthop Res Off Publ Orthop Res Soc 2009;27:540–8. doi:10.1002/jor.20743.
[39] Teeter MG, Milner JS, Naudie DDR, MacDonald SJ. Surface extraction can provide a reference for micro-CT analysis of retrieved total knee implants. The Knee 2014;21:801–5. doi:10.1016/j.knee.2014.04.009.
[40] Galetz MC, Glatzel U. Molecular Deformation Mechanisms in UHMWPE During Tribological Loading in Artificial Joints. Tribol Lett 2010;38:1–13. doi:10.1007/s11249-009-9563-y.
[41] Jin C, Wei W. Wear. In: Narayan R, editor. Biomed. Mater., Springer US; 2009, p. 183–99.
[42] Koji Kato, Koshi Adachi. Wear Mechanisms. Mod. Tribol. Handb. Two Vol. Set, CRC Press; 2000.
[43] Wang A, Stark C, Dumbleton JH. Mechanistic and morphological origins of ultra-high molecular weight polyethylene wear debris in total joint replacement prostheses. Proc Inst Mech Eng [H] 1996;210:141–55.
[44] Nielsen AS, Batchelder DN, Pyrz R. Estimation of crystallinity of isotactic polypropylene using Raman spectroscopy. Polymer 2002;43:2671–6. doi:10.1016/S0032-3861(02)00053-8.
[45] Larkin P. Chapter 1 - Introduction: Infrared and Raman Spectroscopy. In: Larkin P, editor. Infrared Raman Spectrosc., Oxford: Elsevier; 2011, p. 1–5.
[46] Jestel NL. Raman Spectroscopy. In: Bakeev KA, editor. Process Anal. Technol., John Wiley & Sons, Ltd; 2010, p. 195–243.
[47] Affatato S, Grillini L, Battaglia S, Taddei P, Modena E, Sudanese A. Does knee implant size affect wear variability? Tribol Int 2013;66:174–81. doi:10.1016/j.triboint.2013.05.008.
[48] Affatato S, Modena E, Carmignato S, Taddei P. The use of Raman spectroscopy in the analysis of UHMWPE uni-condylar bearing systems after run on a force and displacement control knee simulators. Wear 2013;297:781–90. doi:10.1016/j.wear.2012.10.002.
[49] Barron D, Birkinshaw C. Ultra-high molecular weight polyethylene – Evidence for a three-phase morphology. Polymer 2008;49:3111–5. doi:10.1016/j.polymer.2008.05.004.
[50] Kyomoto M, Miwa Y, Pezzotti G. Strain in UHMWPE for orthopaedic use studied by Raman microprobe spectroscopy. J Biomater Sci Polym Ed 2007;18:165–78.
[51] Lagaron JM, Dixon NM, Reed W, Pastor JM, Kip BJ. Morphological characterisation of the crystalline structure of cold-drawn HDPE used as a model material for the

environmental stress cracking (ESC) phenomenon. Polymer 1999;40:2569–86. doi:10.1016/S0032-3861(98)00500-X.

[52] Lin W, Cossar M, Dang V, Teh J. The application of Raman spectroscopy to three-phase characterization of polyethylene crystallinity. Polym Test 2007;26:814–21. doi:10.1016/j.polymertesting.2007.05.004.

[53] Mirabella FM, Bafna A. Determination of the crystallinity of polyethylene/α-olefin copolymers by thermal analysis: Relationship of the heat of fusion of 100% polyethylene crystal and the density. J Polym Sci Part B Polym Phys 2002;40:1637–43. doi:10.1002/polb.10228.

[54] Naylor CC, Meier RJ, Kip BJ, Williams KPJ, Mason SM, Conroy N, et al. Raman Spectroscopy Employed for the Determination of the Intermediate Phase in Polyethylene. Macromolecules 1995;28:2969–78. doi:10.1021/ma00112a050.

[55] Rull F, Prieto AC, Casado JM, Sobron F, Edwards HGM. Estimation of crystallinity in polyethylene by Raman spectroscopy. J Raman Spectrosc 1993;24:545–50. doi:10.1002/jrs.1250240813.

[56] Taddei P, Di Foggia M, Affatato S. Raman characterisation of conventional and cross-linked polyethylene in acetabular cups run on a hip joint simulator. J Raman Spectrosc 2011;42:1344–52. doi:10.1002/jrs.2867.

[57] Puppulin L, Kumakura T, Yamamoto K, Pezzotti G. Structural profile of ultra-high molecular weight polyethylene in acetabular cups worn on hip simulators characterized by confocal Raman spectroscopy. J Orthop Res Off Publ Orthop Res Soc 2011;29:893–9. doi:10.1002/jor.21331.

[58] Glotin M, Mandelkern L. A Raman spectroscopic study of the morphological structure of the polyethylenes. Colloid Polym Sci 1982;260:182–92. doi:10.1007/BF01465438.

[59] Strobl GR, Hagedorn W. Raman spectroscopic method for determining the crystallinity of polyethylene. J Polym Sci Polym Phys Ed 1978;16:1181–93. doi:10.1002/pol.1978.180160704.

[60] Stuart BH. Introduction. Infrared Spectrosc. Fundam. Appl., John Wiley & Sons, Ltd; 2004, p. 1–13.

[61] Stuart BH. Polymers. Infrared Spectrosc. Fundam. Appl., John Wiley & Sons, Ltd; 2004, p. 113–36.

[62] Kazarian SG, Chan KLA. Applications of ATR-FTIR spectroscopic imaging to biomedical samples. Biochim Biophys Acta BBA - Biomembr 2006;1758:858–67. doi:10.1016/j.bbamem.2006.02.011.

[63] Maria C. Application of FTIR Spectroscopy in Environmental Studies. In: Akhyar Farrukh M, editor. Adv. Asp. Spectrosc., InTech; 2012.

[64] Gulmine JV, Janissek PR, Heise HM, Akcelrud L. Polyethylene characterization by FTIR. Polym Test 2002;21:557–63. doi:10.1016/S0142-9418(01)00124-6.

[65] Stark NM, Matuana LM. Surface chemistry changes of weathered HDPE/wood-flour composites studied by XPS and FTIR spectroscopy. Polym Degrad Stab 2004;86:1–9. doi:10.1016/j.polymdegradstab.2003.11.002.

[66] Pagès P, Carrasco F, Surina J, Colom X. FTIR and DSC study of HDPE structural changes and mechanical properties variation when exposed to weathering aging during canadian winter. J Appl Polym Sci 1996;60:153–9. doi:10.1002/(SICI)1097-4628(19960411)60:2<153::AID-APP2>3.0.CO;2-R.

[67] Kaci M, Sadoun T, Cimmino S. Crystallinity Measurements of Unstabilized and HALS-stabilized LDPE Films Exposed to Natural Weathering by FT-IR, DSC and WAXS Analyses. Int J Polym Anal Charact 2001;6:455–64. doi:10.1080/10236660108033961.
[68] Stuart BH. Spectral Analysis. Infrared Spectrosc. Fundam. Appl., John Wiley & Sons, Ltd; 2004, p. 45–70.
[69] Hagemann H, Snyder RG, Peacock AJ, Mandelkern L. Quantitative infrared methods for the measurement of crystallinity and its temperature dependence: polyethylene. Macromolecules 1989;22:3600–6. doi:10.1021/ma00199a017.
[70] Zerbi G, Gallino G, Del Fanti N, Baini L. Structural depth profiling in polyethylene films by multiple internal reflection infra-red spectroscopy. Polymer 1989;30:2324–7. doi:10.1016/0032-3861(89)90269-3.
[71] Davey SM, Orr JF, Buchanan FJ, Nixon JR, Bennett D. Measurement of Molecular Orientation in Retrieved Ultra-high-molecular-weight Polyethylene (UHMWPE) Hip Sockets using Fourier-transform Infrared Spectroscopy. Strain 2004;40:203–10. doi:10.1111/j.1475-1305.2004.00166.x.
[72] Rueda DR, Hidalgo A, Calleja FJB. An i.r. study of the "amorphous" phase in melt crystallized polyethylene. Spectrochim Acta Part Mol Spectrosc 1978;34:475–80. doi:10.1016/0584-8539(78)80042-7.
[73] Costa L, Jacobson K, Bracco P, Brach del Prever EM. Oxidation of orthopaedic UHMWPE. Biomaterials 2002;23:1613–24.
[74] Wimmer MA, Laurent MP, Haman JD, Jacobs JJ, Galante JO. Surface damage versus tibial polyethylene insert conformity: a retrieval study. Clin Orthop 2012;470:1814–25. doi:10.1007/s11999-012-2274-y.
[75] Wu X. Medial vs. Lateral Thinning in Retrieval Series of Four Knee Designs, 2014, p. 163.
[76] Jacobs JJ, Patterson LM, Skipor AK, Hall DJ, Urban RM, Black J, et al. Postmortem retrieval of total joint replacement components. J Biomed Mater Res 1999;48:385–91.
[77] Rand JA, Ilstrup DM. Survivorship analysis of total knee arthroplasty. Cumulative rates of survival of 9200 total knee arthroplasties. J Bone Jt Surg 1991;73:397–409.
[78] Kurelec L, Rastogi S, Meier RJ, Lemstra PJ. Chain Mobility in Polymer Systems: On the Borderline between Solid and Melt. 3. Phase Transformations in Nascent Ultrahigh Molecular Weight Polyethylene Reactor Powder at Elevated Pressure As Revealed by in Situ Raman Spectroscopy. Macromolecules 2000;33:5593–601. doi:10.1021/ma9911187.
[79] Affatato S, Bersaglia G, Emiliani D, Foltran I, Taddei P, Reggiani M, et al. The performance of gamma- and EtO-sterilised UHMWPE acetabular cups tested under severe simulator conditions. Part 2: wear particle characteristics with isolation protocols. Biomaterials 2003;24:4045–55.
[80] Dothée D, Berjot M, Marx J. Measurement of the degree of crystallinity of polyethylene wear debris by means of Raman spectroscopy. Polym Degrad Stab 1988;20:149–55. doi:10.1016/0141-3910(88)90083-3.
[81] Kim M, Noh J, Chung H. Comparison of near-infrared and Raman spectroscopy for the determination of the density of polyethylene pellets. Anal Chim Acta 2009;632:122–7. doi:10.1016/j.aca.2008.10.057.
[82] Sato H, Shimoyama M, Kamiya T, Amari T, Šašic S, Ninomiya T, et al. Raman spectra of high-density, low-density, and linear low-density polyethylene pellets and prediction of

their physical properties by multivariate data analysis. J Appl Polym Sci 2002;86:443–8. doi:10.1002/app.10999.

[83] Pigeon M, Prud'homme RE, Pezolet M. Characterization of molecular orientation in polyethylene by Raman spectroscopy. Macromolecules 1991;24:5687–94. doi:10.1021/ma00020a032.

[84] Tarantili PA, Andreopoulos AG, Galiotis C. Real-Time Micro-Raman Measurements on Stressed Polyethylene Fibers. 1. Strain Rate Effects and Molecular Stress Redistribution. Macromolecules 1998;31:6964–76. doi:10.1021/ma961498l.

[85] M Kop A, Swarts E. Quantification of polyethylene degradation in mobile bearing knees: A retrieval analysis of the Anterior-Posterior-Glide (APG) and Rotating Platform (RP) Low Contact Stress (LCS) knee. Acta Orthop 2007;78:364–70. doi:10.1080/17453670710013942.

[86] Benjamin J, Szivek J, Dersam G, Persselin S, Johnson R. Linear and volumetric wear of tibial inserts in posterior cruciate-retaining knee arthroplasties. Clin Orthop 2001:131–8.

[87] Engh CA, Zimmerman RL, Hopper RH, Engh GA. Can Microcomputed Tomography Measure Retrieved Polyethylene Wear? Comparing Fixed-bearing and Rotating-platform Knees. Clin Orthop 2013;471:86–93. doi:10.1007/s11999-012-2513-2.

[88] Lavernia CJ, Sierra RJ, Hungerford DS, Krackow K. Activity level and wear in total knee arthroplasty: A study of autopsy retrieved specimens. J Arthroplasty 2001;16:446–53. doi:10.1054/arth.2001.23509.

[89] Teeter MG, Brandt J-M, Naudie DDR, Bohm ER, McCalden RW, Holdsworth DW. Measurements of surface and subsurface damage in retrieved polyethylene tibial inserts of a contemporary design. J Long Term Eff Med Implants 2012;22:21–31.

[90] Teeter MG, Parikh A, Taylor M, Sprague J, Naudie DD. Wear and Creep Behavior of Total Knee Implants Undergoing Wear Testing. J Arthroplasty 2015;30:130–4. doi:10.1016/j.arth.2014.08.001.

[91] Berzins A, Jacobs JJ, Berger R, Ed C, Natarajan R, Andriacchi T, et al. Surface damage in machined ram-extruded and net-shape molded retrieved polyethylene tibial inserts of total knee replacements. J Bone Joint Surg Am 2002;84-A:1534–40.

[92] Andriacchi TP, Stanwyck TS, Galante JO. Knee biomechanics and total knee replacement. J Arthroplasty 1986;1:211–9. doi:10.1016/S0883-5403(86)80033-X.

[93] Currier JH, Bill MA, Mayor MB. Analysis of wear asymmetry in a series of 94 retrieved polyethylene tibial bearings. J Biomech 2005;38:367–75. doi:10.1016/j.jbiomech.2004.02.016.

[94] Hoshino A, Fukuoka Y, Ishida A. Accurate in vivo measurement of polyethylene wear in total knee arthroplasty. J Arthroplasty 2002;17:490–6.

[95] Crowninshield RD, Wimmer MA, Jacobs JJ, Rosenberg AG. Clinical performance of contemporary tibial polyethylene components. J Arthroplasty 2006;21:754–61. doi:10.1016/j.arth.2005.10.012.

[96] Gill HS, Waite JC, Short A, Kellett CF, Price AJ, Murray DW. In vivo measurement of volumetric wear of a total knee replacement. The Knee 2006;13:312–7. doi:10.1016/j.knee.2006.04.001.

[97] Muratoglu OK, Bragdon CR, Jasty M, O'Connor DO, Von Knoch RS, Harris WH. Knee-simulator testing of conventional and cross-linked polyethylene tibial inserts. J Arthroplasty 2004;19:887–97.

[98] T. Schwenke DO. Differences in wear between load and displacement control tested total knee replacements. Wear 2009:757–62. doi:10.1016/j.wear.2009.01.028.
[99] Laurent M. High Cycle Wear of Highly Crosslinked UHMWPE Tibial Articular Surfaces Evaluated in a Knee Simulator, Dallas, Texas, USA: 2002.
[100] Popoola OO, Yao JQ, Johnson TS, Blanchard CR. Wear, delamination, and fatigue resistance of melt-annealed highly crosslinked UHMWPE cruciate-retaining knee inserts under activities of daily living. J Orthop Res Off Publ Orthop Res Soc 2010;28:1120–6. doi:10.1002/jor.21104.
[101] Currier JH. Medial versus Lateral Thinning in Retrieved Knee Bearing: Fixed-Bearing and Mobile-Bearing Wear Differently, Las Vegas, Nevada, USA: 2015.
[102] Minn M, Sinha SK. Molecular Orientation, Crystallinity, and Topographical Changes in Sliding and their Frictional Effects for UHMWPE Film. Tribol Lett 2009;34:133–40. doi:10.1007/s11249-009-9419-5.

VITA

NAME: Elmira Moslemi Rad

EDUCATION: B.S., Chemical Engineering, University of Shiraz, Iran, 2005

M.S., Chemical Engineering, Shahid Bahonar University of Kerman, Iran, 2009

M.S., Bioengineering, University of Illinois at Chicago, Illinois, 2015

ABSTRACTS: Moslemi Rad E, Knowlton CB, Fullum S, Lundberg HJ, Laurent MP, Pourzal R, Wimmer MA: *Is linear penetration an accurate surrogate measure for volumetric wear in TKR tibial liners?*, Rush University Research Symposium, 2015.

Moslemi Rad E, Knowlton CB, Fullum S, Lundberg HJ, Laurent MP, Pourzal R, Wimmer MA: *Is linear penetration an accurate surrogate measure for volumetric wear in TKR tibial liners?*, Orthopedic Research Society, 2015.

Moslemi Rad E, Knowlton CB, Lundberg HJ, Laurent MP, Pourzal R, Wimmer MA. *Wear Assessment of Total Knee replacement Polyethylene Liners retrieved after Revision Surgery,* Oral presentation at the 2nd International Conference on BioTribology, Toronto, Canada. May 2014.

Moslemi Rad E, Knowlton CB, Lundberg HJ, Laurent MP, Pourzal R, Wimmer MA. *Wear Assessment of Total Knee replacement Polyethylene Liners retrieved after Revision Surgery,* Rush University Research Symposium, 2014.